Paleozoic tectonics of the southern Chinese Tianshan: Insights from structural, chronological and geochemical studies of the Heiyingshan ophiolitic mélange (NW China)

Bo Wang, Liangshu S. Shu, Michel Faure, Bor-Ming Jahn, Dominique Cluzel, Jacques Charvet, Sun-Lin Chung, Sébastien Meffre

Paleozoic tectonics of the southern Chinese Tianshan: Insights from structural, chronological and geochemical studies of the Heiyingshan ophiolitic mélange (NW China)

Bo Wang[a, b, c, *], Liangshu Shu[a], Michel Faure[c], Bor-ming Jahn[b], Dominique Cluzel[c, d], Jacques Charvet[c], Sun-lin Chung[e], Sébastien Meffre[f]

[a] *State Key Laboratory for Mineral Deposits Research, School of Earth Sciences and Engineering, Nanjing University, 210093 Nanjing, China*

[b] *Institute of Earth Sciences, Academia Sinica, Taipei, 11529 Taiwan*

[c] *Institut des Sciences de la Terre d'Orléans, UMR CNRS 6113, Université d'Orléans, 1A rue de la Férollerie, 45071 Orléans, France*

[d] *Pole Pluridisciplinaire de la Matière et de l'Environnement, EA 3325, Université de la Nouvelle-Calédonie, 98851 Nouméa, New Caledonia*

[e] *Department of Geological Sciences, National Taiwan University, Taipei, 10617 Taiwan*

[f] *Centre of Excellence in Ore Deposits, University of Tasmania, Hobart Tasmania 7001, Australia*

V9.2

* Corresponding author (B. Wang),

Email: burh_cw@yahoo.com

ABSTRACT

In the southern Chinese Tianshan, the southernmost part of the Central Asian Orogenic Belt (CAOB), widespread ophiolitic mélanges form distinct tectonic units that are crucial for understanding the formation of the CAOB. However, the polarity of oceanic subduction and age of orogeny are still in controversy. In order to better understand these geological problems, a comprehensive study was conducted on the Heiyingshan ophiolitic mélange in SW Chinese Tianshan. Detailed structural analysis reveals that the ophiolitic mélange is tectonically underlain by sheared and weakly metamorphosed pre-Middle Devonian rocks, and unconformably overlain by unmetamorphosed and undeformed lower Carboniferous (Serpukhovian) to Permian strata. Igneous assemblage of the mélange comprises OIB-like alkali basalt and andesite, N-MORB-like tholeiitic basalt, sheeted diabase dike, cumulate gabbro and peridotite. Mafic rocks display supra-subduction signature, and some bear evidence of contamination by continental crust, suggesting a continental marginal (back-arc) basin setting. The gabbro was dated at 392 ± 5 Ma by the zircon U-Pb LA-ICP-MS method. Famennian-Visean radiolarian microfossils were found in the siliceous matrix of the ophiolitic mélange. Mylonitic phyllite yielded muscovite $^{40}Ar/^{39}Ar$ plateau ages of 359 ± 2 Ma and 356 ± 2 Ma.

These new data, combined with previously published results, suggest that the mafic protoliths originally formed in South Tianshan back-arc basin during the late Silurian to Middle Devonian, and were subsequently incorporated into the ophiolitic mélange and thrust northward during the Late Devonian to early Carboniferous. The

opening of the back-arc basin was probably induced by south-dipping subduction of the Paleo-Tianshan Ocean in the early Paleozoic, and the Central Tianshan block was rifted away from the Tarim block. Final closure of the back-arc basin in the early Carboniferous formed the South Tianshan Suture Zone and re-amalgamated the two blocks.

Keywords: Ophiolitic mélange; zircon U-Pb, Ar-Ar and bistratigraphic geochronology; geochemistry; Paleozoic tectonics; back-arc basin; Southern Tianshan (Tien Shan)

1. Introduction

The Tianshan Belt, also known as “Tien Shan” in the literature, constitutes the southwestern part of the Central Asia Orogenic Belt (CAOB) (Fig. 1A) (e.g. Jahn et al., 2000; Jahn, 2004; Xiao et al., 2004; Kröner et al., 2007; Windley et al., 2007) or Altaids (Şengör et al., 1993; Şengör and Natal’in, 1996; Xiao et al., 2010). It is a key area for studying the tectonic evolution of the CAOB, which is one of the world’s most complex and long-lasting accretionary orogens. Formation of the CAOB resulted from the subduction and closure of multiple oceanic basins in the broad, SW Pacific-type Paleo-Asian Ocean (Khain et al., 2003), and subsequent amalgamation of various microcontinents, magmatic arcs and accretionary complexes between the Tarim-North China and Siberian cratons (e.g. Coleman, 1989; Shu et al., 2002; Charvet et al., 2007; Kröner et al., 2007; Windley et al., 2007).

Tectonic reconstruction of an accretionary orogen requires a good understanding of suture zones which generally contain ophiolitic mélanges. In the southwestern Chinese Tianshan, several mélange belts have been recognized (e.g. Xiao et al., 1990, 1992; Gao et al., 1998) (Fig. 1C), and studied for their petrological and geochemical characteristics, emplacement times and tectonic significance (Jiang and Li, 1990; Gao et al., 1995a; Tang et al., 1995; Wang et al., 1995b; Liu, 2001; Zhou et al., 2004; Dong et al., 2005, 2006; Yang et al., 2005; Long et al., 2006; Ma et al., 2006a; Charvet et al., 2007; Shu et al., 2007; Zhu, 2007). However, due to the limited amount of data, it remains difficult to: (1) correlate them laterally; (2) establish the timing and kinematics of their tectonic emplacement; (3) reconstruct the geodynamic evolution of the southern Tianshan Belt. Consequently, two key issues related to tectonics of the southern Chinese Tianshan are still in debate. The first one is the age of the orogeny which some authors considered as to be late Paleozoic (e.g., Gao et al., 1998, 2009; Wang et al., 2010) but, alternatively, others ague for Triassic (e.g., Zhang et al., 2007; Xiao et al., 2008). The second issue concerns the polarity of subduction of the paleo-Tianshan Ocean, a north-directed subduction was proposed by Windley et al. (1990), Xiao et al. (2004, 2008), Gao et al. (1998) and Gao and Klemd (2003); whereas, a southward subdution is more likely consistent with newly published data (Charvet et al., 2007; Wang et al., 2008; Lin et al., 2009); and a compromise of bi-directional subduction was suggested by Gao et al. (2009).

In order to put more constraints on the kinematics and age of orogenic event, we conducted a comprehensive study on ophiolitic mélange in the Heiyingshan section

(Figs. 1B and 2), southern Chinese Tianshan. The data set includes field structural observation, dating of the ophiolitic blocks and matrix using zircon U-Pb, muscovite $^{40}Ar/^{39}Ar$, and paleontological methods, as well as whole-rock and Sr-Nd isotopic geochemistry of the magmatic rocks. The new and literature data are then used to discuss the geological significance of the ophiolitic mélange and the tectonic evolution of the southern Chinese Tianshan.

2. Geological background

The Chinese Tianshan is the eastern segment of the Tianshan Belt that extends E-W for more than 2,500 km from China to Central Asian territories (Fig. 1C). It is divided into northern and southern ranges by the Kazakh-Yili and Tu-Ha basins (Fig. 1C). The southern Chinese Tianshan of this study refers to the mountain ranges situated between the Yining and Tarim Cenozoic basins (Fig. 1B). This area can be subdivided into three domains by a high-pressure (HP) metamorphic belt and southern Tianshan ophiolitic mélange zones. These domains are, from north to south: (1) the Yili-North Tianshan magmatic arc, (2) the Central Tianshan Paleozoic succession, and (3) the northern Tarim margin.

2.1. HP metamorphic complex and related ophiolitic rocks

A HP metamorphic belt is exposed to the south of the Nalati Fault (fault 1 in Fig. 1B). This belt consists of greenschist-, blueschist- and eclogite-facies rocks, which were probably transformed from sea-floor deposits and basaltic rocks (Gao et al.,

1995b, 1999; Ai et al., 2006). Isotopic ages of 415-343 Ma (phengite $^{40}Ar/^{39}Ar$ plateau and Sm-Nd isochron) were obtained for eclogite and blueschist (Dobretsov et al., 1987; Xiao et al., 1992; Gao et al., 1995b, 2000, 2006; Gao and Klemd, 2003), and the peak HP metamorphism was considered to have occurred at ~345 Ma (Gao and Klemd, 2003; Klemd et al., 2005). In addition, eclogites and blueschists yielded younger ages of 331~302 Ma (recrystallized phengite $^{40}Ar/^{39}Ar$ plateau and Rb-Sr isochron) that were regarded as reflecting the timing of retrograde metamorphism during exhumation of the HP metamorphic rocks (Gao and Klemd, 2003; Stupakov et al., 2004; Klemd et al., 2005; Simonov et al., 2008; Wang et al., 2010).

Ophiolite relics occur sporadically within the HP metamorphic belt. In the Dalubayi ophiolite (locality "d" in Fig. 1B), OIB-like gabbro and basalt were dated at 600 ± 15 Ma and 590 ± 11 Ma (zircon U-Pb), respectively (Yang et al., 2005; Zhu, 2007). In Xiate (locality "x" in Fig. 1B), an age of 516 ± 7 Ma was obtained for MORB-type basalt (zircon U-Pb SHRIMP) (Qian et al., 2009). In the Mishigou and Gangou areas (localities "m" and "g" in Fig. 1B), a meta-basaltic rock (Laurent-Charvet et al., 2001; Liu et al., 2005; Charvet et al., 2007) was dated at ca. 345 Ma (phengite $^{40}Ar/^{39}Ar$; Liu and Qian, 2003).

2.2. Southern Tianshan ophiolitic melange zones

To the south, 70-100 km away from the HP metamorphic belt, several ophiolitic mélange zones occur discontinuously in the areas of Aheqi, Heiyingshan, Serikeya, Kulehu, Wuwamen, Yushugou and Tonghuashan (localities "a", "h", "s", "k", "w",

"y" and "t" in Fig. 1B, respectively). Near Aheqi, mafic lavas with geochemical affinity for P-MORB yielded a Sm-Nd isochron age of 392 ± 15 Ma (Xu et al., 2003). In the Kulehu mélange, an N-MORB pillowed basalt was dated at 425 ± 8 Ma (zircon U-Pb SHRIMP; Long et al., 2006), and a quartz schist gave a biotite $^{40}Ar/^{39}Ar$ plateau age of 370 ± 5 Ma, which was interpreted as the time of shearing of the highly deformed matrix of the mélange (Cai et al., 1996). The mélange was later subject to a thermal overprint at 259 ± 3 Ma (biotite $^{40}Ar/^{39}Ar$ age at a temperature of 260-300 ºC) (Cai et al., 1996). A mylonitic quartzite that is tectonically overlain by the mélange was metamorphosed at 368 ± 1 Ma (muscovite $^{40}Ar/^{39}Ar$ plateau age; Li et al., 2004).

In Yushugou, a cumulate gabbro yielded a zircon U-Pb age of 378 ± 6 Ma (Jiang and Li, 1990; Jiang et al., 2000); a granulite-facies metabasalt (Shu et al., 1996, 2004) yielded zircon U-Pb SHRIMP ages of 392-390 Ma (Zhou et al., 2004), and Ca-amphibole $^{40}Ar/^{39}Ar$ plateau ages of 368-360 Ma (Wang et al., 2003). In the Wuwamen mélange, tholeiitic basalts have geochemical features of N-MORB (Dong et al., 2005). In the Tonghuashan mélange, a gabbro was dated at 420 ± 14 Ma by the amphibole K-Ar method (Zhang and Wu, 1985); blueschist-facies metamorphic rocks (Gao et al., 1993) yielded a glaucophane $^{40}Ar/^{39}Ar$ age of ca. 360 Ma (Liu and Qian, 2003).

Middle Devonian (Givetian) to early Carboniferous (Tournaisian or Visean) radiolarian and conodont microfossils were found in abundance in cherts of the Kulehu and Heiyingshan mélanges (Gao et al., 1998; Liu, 2001; Zhu, 2007). Early-Middle Devonian radiolarian fossils were also identified in chert blocks in the

Tonghuashan mélange (Gao et al., 1998).

Moreover, according to recently compiled geological map (Apayarov et al., 2008), in the southern Kyrgyzstan Tianshan, early Paleozoic serpentinite, peridotite and gabbro are accompanied with middle Silurian-Carboniferous (?) basalt, spilite, chert, shale and siltstone. However, their structure, age and geochemical significance remain unknown.

2.3. Yili-North Tianshan magmatic arc

This domain corresponds to the Bogda-North Tianshan arc in the eastern Tianshan (Charvet et al., 2007), and the "Kazakh (northern Tien Shan) - Yili Plate" in Kazakhstan and Kyrgyzstan (Mikolaichuk et al., 1995; Konopelko et al., 2008; Gao et al., 2009). The magmatic arc comprises Late Devonian to Carboniferous shallow marine and terrigenous sedimentary rocks, calc-alkaline volcanic rocks (363-313 Ma) and I-type granites (370-308 Ma) (e.g., XBGMR, 1993; Zhu et al., 2005, 2006a, 2006b; Wang et al., 2006, 2007a, 2007b; Xu et al., 2006; Gao et al., 2009). In addition, Silurian to Middle Devonian (436-398 Ma) and minor Ordovician (479-466 Ma) intrusive rocks occur along the Nalati Fault (Zhu et al., 2006c; Konopelko et al., 2008; Gao et al., 2009; Yang and Zhou, 2009). In the Yili area, a Precambrian metamorphic complex occurs beneath the arc series and is composed of Neoproterozoic gneissic granites, a series of presumed Mesoproterozoic metasedimentary rocks, and a presumed Paleoproterozoic crystalline basement (e.g., XBGMR, 1993; Allen et al., 1993; Gao et al., 1998; Hu et al., 2006).

2.4. Central Tianshan Paleozoic succession and Proterozoic substratum

This domain refers to the area located in the Hark Shan and extends eastward to the Erbin Shan and Baluntai areas (Fig. 1B; Charvet et al., 2007; Wang et al., 2008). The Hark Shan is mainly made up of Ordovician to Silurian marble, dolomite, crystalline limestone with interbeded breccia and clastic rocks (XBGMR, 1993; Wang et al., 1997; Zhou et al., 2001). Late Silurian to Devonian deformed turbidite, shallow-water to deep marine clastic rocks, carbonate and chert are observed in the south of the Kulehu area (locality "k" in Fig. 1B) (Zhou et al., 2001; Zhu, 2007). The Carboniferous series consists of undeformed clastic rocks and limestone without volcanic rocks. An unconformity occurs between the Carboniferous and older rocks (XBGMR, 1993).

Arc-type intermediate to felsic volcanic and volcaniclastic rocks of mostly Ordovician-late Silurian age were recognized in this domain. In the Aheqi area (locality "a" in Fig. 1B), a calc-alkaline andesite yielded a $^{40}Ar/^{39}Ar$ whole-rock isochron age of 427 ± 5 Ma (Gong et al., 2003). Immediately to the south of the HP metamorphic belt, a rhyolite was dated at ca. 396 Ma (zircon U-Pb age; Zhu, 2007). Ordovician to Silurian weakly deformed volcanic rocks occur in the south of the Nalati Pass and in the Mishigou area (localities "n" and "m" in Fig. 1B, respectively) (Ma et al., 2006b; Charvet et al., 2007). Recent study on detrital zircons and paleocurrent in Silurian-Devonian clastic rocks from the Biediele area (locality "b" in Fig. 1B) suggests that plenty of Early Devonian (~415 Ma) magmatic zircons

originated from Tarim (Luo et al., 2010).

Early-middle Paleozoic arc-type granitoids are widely distributed in this domain. They include granodiorite of the Bayinbulak area (447 ± 1 Ma), granites north of Kulehu (dated at 426-425 Ma by the multigrain zircon U-Pb TIMS method; Xu et al., 2006), gabbro and granodiorite between Mishigou and Yushugou (dated at 428-394 Ma by the zircon U-Pb, SHRIMP and TIMS methods; Hopson et al., 1989; Shi et al., 2007; Xu et al., 2006; Yang and Wang, 2006; Yang et al., 2006) (Fig. 1B).

Moreover, A-type granites (470-420 Ma, zircon U-Pb ages) were recognized in this domain. The occurrence of such granite suggests that an extensional regime probably existed during the Middle Ordovician to late Silurian (Han et al., 2004). Furthermore, north of Kumux, Late Devonian granites (368-361 Ma, zircon U-Pb SHRIMP) show geochemical and isotopic features indicative of a syn-collisional tectonic setting (Shi et al., 2007). In the Kumux and Wuwamen areas (Fig. 1B), late Carboniferous granites (327-297 Ma, zircon U-Pb TIMS) formed in a post-collisional setting (Xu et al., 2006; Zhu et al., 2008a).

The Proterozoic rocks are mainly exposed in the Baluntai area (Fig. 1B) where an orthogneiss was dated at ~700 Ma by zircon SHRIMP U-Pb method (Yang et al., 2006; Zhu and Song, 2006). In addition, to the north of Kulehu (Figs. 1B, 2) a Neoproterozoic pegmatite was dated at ~931 Ma by zircon U-Pb method (Xinjiang Bureau of 305 Project, unpublished data); migmatite, marble and metasediments are of probable Precambrian in age on the basis of occurrence of acritarchs *Brocholaminaria nigrita* in a limestone and a whole-rock Rb-Sr isochron age of 606 ±

4 Ma on a quartz schist (Wang et al., 1995; 1996). These Precambrian rocks are comparable to coeval rocks of the Tarim block (Hu et al., 2006; Lu et al., 2008), but are separated from the Tarim basement by the southern Tianshan ophiolitic mélange zones (Fig. 1B). This domain is therefore interpreted as an early Paleozoic continental-based magmatic arc of the Central Tianshan (Charvet et al., 2007; Wang et al., 2008) rather than a passive margin of northern Tarim (e.g. Chen et al., 1999; Carroll et al., 2001).

2.5. Northern Tarim margin

The Paleozoic of this domain is distinct from that of the Central Tianshan in lithologic and tectono-metamorphic features (Wang et al., 2008). To the southwest of Akesu and southeast of Korla (Fig. 1B), late Cambrian to Middle Devonian strata are composed of non-metamorphic, gently folded marine carbonate and continental sandstone, unconformably overlain by late Paleozoic to Mesozoic rocks (e.g. XBGMR, 1993; Carroll et al., 1995, 2001). The basement is composed of Archean to Proterozoic amphibolite and orthogneiss, which occur in the Kuluketage area (e.g., Hu et al., 2006; Lu et al., 2008). Neoproterozoic carbonate and Neoproterozoic blueschists crop out in the Akesu area (XBGMR, 1993; Liou et al., 1996).

To the south of Serikeya and Kulehu (Fig. 1B), Late Devonian calc-alkaline diorite (382 ± 6 Ma, zircon U-Pb SHRIMP), granodiorite and monzonite are considered to have formed along an active margin (Zhu et al., 2008b). Near Korla, gabbro, diorite, quartz diorite and granite also show calc-alkaline geochemical

features. The granite yielded a zircon U-Pb age of 363 ± 2 Ma (Jiang et al., 2001). Moreover, Late Devonian arc-type volcanic rocks developed in the northern Kuluketage area (Fig. 1B) (Ma et al., 2002).

In Kyrgyz southern Tianshan, Cambrian-Ordovician basalt, andesite, lava breccia, tuff and Middle Ordovician diorite, granodiorite and granite occur to the south of the Atbashy belt (Apayarov et al., 2008). More to the south, late Silurian to Early Devonian trachyrhyolite and tuff are associated with limestone and terrigenous clastic rocks (Apayarov et al., 2008).

3. Structure of the Heiyingshan ophiolitic mélange

Ophiolitic rocks and Paleozoic strata as well as Proterozoic rocks in the southern Tianshan are all involved in NE-SW trending, SE-verging folds, and NW to N-dipping high angle reverse faults (Figs. 1 and 2). These structures also affected Mesozoic and Cenozoic rocks of the northern Tarim basin, and are consistent with deformation style of the Kuqa foreland fold-and-thrust belt (e.g. Lu et al., 1994; Allen et al., 1999) which was produced by Cenozoic NW-SE shortening due to the Indo-Eurasia collision (e.g. Hendrix et al., 1994). Three litho-tectonic units are cross-cut and placed into contact by north-dipping brittle faults (Figs. 2A and 2B); they are: the upper unit, the ophiolitic mélange and the lower unit discussed in more detail below.

3.1. The upper unit

This unit is composed of Carboniferous basal conglomerate, sandstone and

bioclastic limestone, Early Permian basalt and rhyolite, and Middle Permian to Jurassic terrigenous carbonaceous rocks. These strata occur mainly to the south of the ophiolitic mélange. Early Carboniferous (Serpukhovian) sandstone and limestone bearing *Gigantoproductus* and *Lithostrotion* unconformably overlie the ophiolitic mélange as well as Early Paleozoic rocks (Fig. 2; XBGMR, 1983). This unit and overlying Tertiary rocks were deformed by a series of SE-verging open folds (Fig. 2B) which are attributed to the Cenozoic deformation.

3.2. The ophiolitic mélange

This mélange is exposed as discontinuous lenses sliced up by brittle faults (Fig. 2B). Magmatic rocks include peridotite, cumulate gabbro, and massive or pillowed basalt (Fig. 3A). Sheeted diabase dikes also occur but are laterally discontinuous and bound by sheared peridotite (Fig. 3B), indicating a blocky nature. The thickness of diabase dykes ranges from several tens of centimeters to a few meters. Peridotite is strongly serpentinized and crosscut by calcite veins (Fig. 3C). Blocks of radiolarian chert, limestone and sandstone display variable sizes ranging from tens of centimeters to several hundreds of meters; bedding is well preserved in sandstone and limestone blocks that may be confused with the sedimentary matrix; however, the lensoid geometry and changing attitude of the bedding comply with a blocky nature of these rocks. Limestone also occurs as olistoliths in a crushed sedimentary matrix (Fig. 3D), suggesting possible syntectonic sedimentation and subsequent deformation. Pebbly mudstones (Fig. 3E) are locally recognized and indicate a mass-flow deposition. The

sedimentary matrix is composed of laminated calcareous turbidite and siliceous mudstone, both are often folded and boudinaged (Fig. 3F). In most cases the matrix is strongly sheared or even mylonitized so that a scaly fabric is developed in weakly metamorphosed pelite (Fig. 3G). Planar structures such as bedding or cleavage have an average strike of N40°E but, due to later folding, the dip may be either northward or southward (inset of Fig. 2A).

3.3. The lower unit

This unit is composed of strongly deformed Ordovician to Silurian limestone, marble and sandstone, and the underlying metamorphic rocks including amphibolite, biotite gneiss, cordierite-quartz schist, micaschist and actinolite schist (XBGMR, 1983; Wang et al., 1997; Zhu, 2007). The metamorphic rocks were previously assigned to the lower Paleozoic, but their protoliths could be older than ~600 Ma and underwent multiphase deformation and metamorphism during ~606 Ma (whole-rock Rb-Sr isochron age on a quartz schist; Wang et al., 1995a, 1996), 370-336 Ma and ~260 Ma (biotite $^{40}Ar/^{39}Ar$ plateau ages on quartz schist; Wang et al., 1995a). The lower unit and ophiolitic mélange are intruded by Early Permian (275-273 Ma; Liu et al., 2004) stitching granitic plutons (Fig. 2).

3.4. North-directed ductile thrusting in the mélange and lower unit

Although has been extensively overprinted by south-vergent folding and faulting, an earlier ductile deformation can be recognized in pre-Visean rocks. Marble and

clastic rocks in the lower unit show a gently south-dipping slaty cleavage and local mylonitic foliation (Figs. 2B and 3H). The planar fabric is a composite bedding-foliation surface that occasionally contains a N-S to NW-SE trending mineral or stretching lineation and intrafolial folds, suggesting intense ductile shearing. Both foliation and lineation were re-deformed by south-verging folding. Due to intense strain and prominent recrystallization, kinematic indicators related to the sub-meridian lineation are generally difficult to identify. However, locally, fibrous quartz or calcite pressure shadows crystallized around sigmoid limestone clasts within the sheared matrix and demonstrate a top-to-the north sense of shear (Fig. 3G).

Similar ductile deformation can be recognized throughout the southern Chinese Tianshan. In Kulehu mélange, kinematic criteria, such as sigmoidal clasts of volcanic rocks, sheared bands within the matrix (Fig. 4A) and intrafolial asymmetric folds (Fig. 4B), indicate a north-directed ductile thrusting. All these fabrics were involved in subsequent south-verging brittle folds and thrusts (Fig. 4B). In the Biediele area (locality “b” in Fig. 1B), Silurian and Devonian rocks consist of schistose clastic, volcaniclastic rocks and mylonitic marble (Fig. 4C). In the schistose clastic rocks, asymmetric quartz fibers around pyrite grains, sigmoid clasts and drag folds consistently indicate top-to-the-north shearing (Figs. 4D and 4E). These observations are consistent with the kinematics in the Yushugou mélange (Fig. 1B) where ductile deformation produced a flat-lying foliation and a sub-meridian stretching lineation in the matrix and, to a lesser extent, in some of the blocks. Pressure shadows, sigmoid quartz veins or shear bands also indicate top-to-the-north ductile shearing (Fig. 4F)

which may be related to the emplacement of the ophiolitic mélange (Shu et al., 1996; Charvet et al., 2007).

4. Petrography of the magmatic rocks

Peridotite is usually sheared and altered into serpentinite and listwaenite. Dunite is the main type of mantle rock, and it comprises more than 95% olivine, ~2% Cr-spinel and 2-3% magnetite. Olivine is serpentinized, and Cr-spinel has a vermicular habit surrounded by magnetite or set in neoblasts (Fig. 8A). Harzburgite consists of olivine (>70%), orthopyroxene (~25%) and Cr-spinel (<5%). Lherzolite contains olivine (~70%), orthopyroxene (15-20%), clinopyroxene (5-10%), amphibole (<5%) and spinel (<5%). Secondary carbonate is well developed in all ultramafic rocks.

Gabbro is often coarse-grained and locally shows a cumulate texture (Fig. 8B). Main minerals include plagioclase (~60%), clinopyroxene (~30%), amphibole (~5%) and minor olivine (<5%). Diabase is composed of calcic plagioclase, clinopyroxene and Fe/Ti-oxide. Clinopyroxene is partially replaced by chlorite and/or epidote.

Basalt occurs as massive flows or as pillow lava. The size of pillow varies from 20 to 50 cm in diameter (Fig. 3A). Some basalt and basaltic andesite display porphyritic texture defined by matrix (>50%) and embedded phenocrysts (30-40%) of clinopyroxene, plagioclase, and subordinate olivine and hornblende. The matrix shows a glass-rich hyalopilitic texture that is characteristic of a sub-crystalline groundmass made up of microcrystals of plagioclase, pyroxene and glass (Fig. 8C). In

some cases volcanic rocks also show an aphyritic texture consisting of plagioclase, pyroxene and oxide (Fig. 8D). Most volcanic rocks were subjected to different degrees of alteration, showing replacement of pyroxene by chlorite, epidote and Fe/Ti oxide (Figs. 8C and 8D), and plagioclase by calcite.

5. Sampling and analytical methods for geochronology and geochemistry

A cumulate gabbro (sample 499-11) was collected from the Heiyingshan ophiolitic mélange (GPS: N42º13.34', E82º 13.37'). Zircon grains were extracted from this sample by crushing, sieving, heavy liquids and magnetic separation, and finally by handpicking under binocular microscope. Zircon grains are euhedral, colorless and without fracture. U-Pb dating was carried out at the Radiochronology Laboratory of the Centre of Excellence in Ore Deposits, University of Tasmania, Australia, using a Hewlett Packard HP 4500 quadrupole Inductively Coupled Plasma Mass Spectrometer fitted with a 213 nm NewWave Merchantek UP213 Nd-YAG Laser.

Metapelites (samples 437 and 438-1) were collected from the mylonitic matrix of the mélange (GPS: N42º14.09', E82º 12.52'). Fine-grained muscovite was carefully handpicked under a binocular zoom microscope from ~0.3 mm-size fraction of crushed rock, following thorough ultrasonic rinsing in distilled water. $^{40}Ar/^{39}Ar$ step-heating of muscovite was conducted at the Institute of Geology, Chinese Academy of Geological Sciences (IG-CAGS, Beijing). The detailed analytical technique and procedures were described by Chen and Liu (2002).

Four siliceous mudstone samples (506-1, 506-2, 511 and 512) were collected from the matrix of the mélange (GPS: N42º12.68', E82º13.66'), and were analyzed for microfossils at Nanjing Institute of Geology and Paleontology, Chinese Academy of Sciences (NIGP-CAS).

Two peritotites, one cumulate gabbro, six basalts and one andesite were analyzed for whole rock chemical compositions. Major elements were determined by X-ray fluorescence (XRF) at the Modern Analysis Center, Nanjing University, following procedures described by Couture et al. (1993). Rare earth and other trace elements were analyzed in the State Key Laboratory for Mineral Deposits Research of Nanjing University using a HR-ICP-MS (Finnigan Element II). The analytical technique was described by Gao et al. (2003). A duplication of REE and trace element abundances of the mafic-andesitic rocks and sample 499-3 was performed by an ICP-MS method at the Department of Geological Sciences, National Taiwan University (Taipei), using an Agilent 7500s quadrupole ICP-MS. Details of the analytical procedures may be found in Yang et al. (2005). Analytical errors are 0.5-3% for major elements and 0.7-5% for most REE and trace elements.

Sr and Nd isotopic compositions were determined for the basaltic rocks and andesite using a 7-collector Finnigan MAT-262 mass spectrometer at the Institute of Earth Sciences, Academia Sinica (Taipei). Procedures of chemical separation and analysis were described by Jahn et al. (2009).

6. Dating results

6.1. Zircon U-Pb age of gabbro

The U-Pb isotopic results of the gabbro sample 499-11 are presented in Table 1 and are plotted in a Tera-Wasserburg diagram (Fig. 5). Although cathode luminescence image is not available, the analyzed zircons could be considered as of a magmatic origin on the basis of their euhedral shape and Th/U ratios (>0.1; Table 1) (Vavra et al., 1996). Apparent $^{206}Pb/^{238}U$ ages are more concordant than $^{207}Pb/^{206}U$ ages, and are therefore used to calculate an averaged $^{206}Pb/^{238}U$ age at 392 ± 5 Ma (MSWD = 1.8) from nine analyses that are consistent within errors. This age is interpreted as the crystallization age of the gabbro. Two additional grains give ages of 419 ± 4 Ma and 434 ± 6 Ma, which are consistent with the age of MORB-type basalt (425 ± 5 Ma) in adjacent Kulehu ophilitic mélange (Long et al., 2006). Thus, although other possibilities could not be precluded, these two ages are preferably interpreted here as the age of an earlier stage of magmatism.

6.2. $^{40}Ar/^{39}Ar$ ages of mylonitic metapelite

The $^{40}Ar/^{39}Ar$ dating results are shown in Table 2 and are further illustrated in Fig. 6. The errors represent 2 sigma deviation for plateau ages. For sample 437, eight steps from 500ºC to 1200ºC with 96.9% of ^{39}Ar release yielded a well defined plateau age at 359 ± 2 Ma (MSWD = 0.45). For sample 438-1, a plateau age of 356 ± 2 Ma (MSWD = 0.77) was defined by five contiguous steps from 900ºC through 1300ºC with 87.3% of ^{39}Ar release. The two $^{40}Ar/^{39}Ar$ ages are consistent and hence interpreted as the crystallization time of muscovite during the mylonitization.

6.3. Biostratigraphic constraints on matrix of mélange

The Heiyingshan ophiolitic mélange was previously assigned to the upper Silurian to Lower Devonian Aertengkesi Formation on the basis of coral, brachiopods, gastropods and crinoid fossils found in blocks of limestone and sandstone (XBGMR, 1983). However, the ages of these blocks are often older than mélange, and the age of mélange could be constrained by matrix. In our samples of siliceous mudstone, abundant radiolarian fossils were determined, including *Archocyrtium cf. procerum Cheng, Archocyrtium venustum Cheng, Archocyrtium cf. ludicrum Deflandre, Archocyrtium cf. mirousi Gourmelon, Trilonche almae (Won), Stigmosphaerostylus Pantotolma Braun, Stigmosphaerostylus vulgaris Won, Stigmosphaerostylus wuppertalensis Won), Stigmosphaerostylus cf. Tortispina Ormiston et Lane, Holoeciscus foremanae sp., Albaillella paradoxa sp*. These microfossils are common elements in the *Holoeciscus foremanae* and *Albaillella paradoxa* assemblages of Famennian and Visean ages, respectively. Representative radiolarian species and their occurrence epochs are shown in Fig. 7. This age is consistent with that derived from a radiolarian chert to the northeast of Heiyingshan (Fig. 2A) (Liu, 2001). Thus, early Carboniferous (Visean) represents the upper limit for the formation age of the mélange.

7. Geochemical and isotopic compositions of the magmatic rocks

7.1. Major elements

The results of geochemical analyses are shown in Table 3. Two peridotites show low CaO (0.1-2.2%) and high Mg# values (0.87-0.92). The gabbro has a moderately high Mg# value (0.84), and high abundances of Al_2O_3 (19.4%) and CaO (10.2%), consistent with its cumulate origin.

The basaltic rocks can be subdivided into two groups: tholeiitic and alkali basalt (Fig. 9). The tholeiitic basalts (samples 499-3, 499-6 and pillow basalt sample 499-8) have low contents of K_2O (0.3-1.2%), TiO_2 (0.5-0.6%), and high Mg# values (0.64-0.67). The alkali basalts (samples 499-7, 499-9 and 499-10) are characterized by relatively abundant K_2O (2.0-3.8%), TiO_2 (2.4-2.8%), and low MgO (1.7-2.2%). The andesite (sample 499-4) is characterized by a high Mg# value (0.72) and low Al_2O_3 content with respect to the normal calc-alkaline andesite (Table 3; Wilson, 1989).

Except for the alkali basalt, the tholeiitic basalt, andesite and intrusive rocks show high loss on ignition values (LOI>4.6%; Table 3), which probably resulted from post-magmatic fluid-rock interaction forming carbonate veins and low temperature minerals. Such alteration may have mobilized most major elements and some LIL elements such as Ba, Rb, Sr, U and K that, as a consequence, vary widely in composition (Table 3). However, HFS elements such as Nb, Ta, Zr, Hf, Th and Y, are “immobile” during alteration and therefore are consistent in composition within subgroup (Table 3). Thus, only “immobile” incompatible trace elements and REE are presented below and are used in the following discussion for petrogenesis and tectonic setting of these magmatic rocks.

7.2. REE and Trace elements

The peridotites are typically rich in Ni and Cr, and depleted in REE and high field strength (HFS) elements compared to the Primitive Mantle (<0.1×PM) (Sun and McDonough, 1989) (Table 3). The gabbro is also poor in HFS elements and REE (2× C1 abundances), a feature consistent with its cumulate character. The REE pattern has a slightly negative slope and displays a strong positive Eu anomaly (Eu/Eu* = 1.8), which is likely due to plagioclase accumulation. In multi-element variation diagrams, the negative anomalies in Nb, Ta, and Hf may be a feature of the source or, alternatively, due to accessory mineral fractionation (Figs. 10A and 10B; Table 3).

The tholeiitic basalts show consistently LREE-depleted patterns (La_N/Sm_N = 0.4-0.6, La_N/Yb_N = 0.3-0.5), similar to N-MORB, only lower in total REE abundance (Fig. 10A). Thus, they were likely generated by melting of a highly depleted upper mantle source. In multi-element variation diagrams (Fig. 10B), weak depletion in Nb, Ta and Zr, Hf and positive Eu anomalies (Eu_N/Eu^* = 1.0-1.2) can be observed. These features are distinct from those of the typical N-MORB (Fig. 10B).

The alkali basalts display LREE-enriched patterns (La_N/Sm_N = 3.3-3.4, La_N/Yb_N = 8.6-8.9) (Table 3) which are similar to that of OIB but HREE are less fractionated (Fig. 10C). In the multi-element variation diagram (Fig. 10D) the alkali basalts demonstrate a pronounced depletion in Nb and Ta as compared to typical OIB. Note that both the tholeiitic and alkali basalts have relatively high Th contents (Fig. 10).

The andesite has REE and multi-element variation patterns similar to the alkali basalts. A well marked negative Eu anomaly indicates a fractionated character (Figs.

10C and 10D). However, its lower total REE abundance than alkali basalts in spite of a higher SiO_2 content suggests that the andesite is unlikely to be genetic with the alkali basalts.

7.3. Sr-Nd isotopic compositions

Sr-Nd isotopic data are reported in Table 4. Initial $\varepsilon Nd_{(t)}$ values are calculated using the age of the gabbro (~395 Ma), assuming that it is more or less contemporaneous with the extrusive rocks. The tholeiitic basalts have $\varepsilon Nd_{(395)}$ values ranging from +7.2 to +10.7. Their high $ISr_{(395)}$ values (0.7070-0.7084) are probably related to incorporation of radiogenic Sr during alteration (Jahn et al., 1980; Fig. 11). In contrast, the alkali basalts show negative $\varepsilon Nd_{(395)}$ values (-3.7 to -3.9), but their $ISr_{(395)}$ values (0.7073 to 0.7075) are similar to those of the tholeiites, and this feature may also have resulted from alteration. The andesite sample has an $\varepsilon Nd_{(395)}$ of -4.7 and $ISr_{(395)} = 0.7064$.

Single-stage Nd depleted mantle model ages (t_{DM-1}) vary from ~1450 Ma to ~1470 Ma for the alkali basalts and ca. 1660 Ma for the andesite (Table 4). The fractionation factors ($f_{Sm/Nd}$) of the alkali basalts (-0.39) and andesite (-0.35) are very close to that of the average continental crust (ca. -0.4). The model ages t_{DM-1} of the tholeiitic basalts cannot be calculated as their $f_{Sm/Nd}$ values are too close to that of the depleted mantle.

8. Discussion

8.1. Origin and tectonic setting of the magmatic rocks

The ultramafic and mafic rocks in the Heiyingshan mélange are tectonically associated with chert and limestone, forming a dismembered ophiolite suite. However, the geochemical and isotopic data suggest that the mafic rocks originated from different sources. The tholeiitic basalts have N-MORB REE patterns, trace element abundances, and positive $\varepsilon Nd_{(T)}$ values close to that of present-day depleted mantle. They also show trace element ratios (Zr/Nb = 24-46, Zr/Hf = 29-31 and Nb/Ta = 13-14; Table 3) similar to N-MORB (~30, ~36 and 6-14, respectively; Rollinson, 1993), and plot in the field of N-MORB in the Nb-Zr-Y diagram (Meschede, 1986; Fig. 12A). Therefore, they were most probably produced from a depleted mantle source.

Taking into account the occurrence of pillowed lava, the ophiolitic suite is likely to represent an oceanic crust. The associated dunite, harzburgite and minor lherzolite may thus be remnants of the oceanic lower crust and upper mantle. Some of the ultramafic rocks could have been generated by a relatively high degree of partial melting and fractionation of the upper mantle (Bodinier and Godard, 2004).

The low content of incompatible elements in the tholeiitic basalts is consistent with an already depleted mantle source or, alternatively, is due to a high degree of hydrous melting. This is corroborated by the weak Nb and Ta (and Ti) negative anomalies (Fig. 10B), indicating that the source contained Nb-Ta retaining refractory minerals (ilmenite, pargasitic amphibole) which are generally present in metasomatised (e.g. hydrous) mantle sources. Such features are frequently related to a

supra-subduction setting where the residual depleted mantle was metasomatized by slab-derived fluids (Hawkins, 2003; Kim et al., 2003).

In addition, a high Th content in the tholeiitic basalts may have resulted from contamination with continental crust. Thus, the tholeittic basalts were likely generated during the early stage of continental back-arc basin opening rather than in a fore arc basin (Wilson, 1989; Metcalf and Shervais, 2008; Fig. 12B). Although no isotopic data are available for the gabbro due to its low Nd content, this rocks shows a geochemical affinity to E-MORB (Fig. 12A), suggesting that it probably formed during a later stage of back-arc spreading (Fig. 12B).

In contrast, the alkali basalts and andesite have negative $\varepsilon Nd_{(t)}$ values, indicating that they contain an enriched mantle or lower continental crust component (Rollinson, 1993). Their Nd depleted mantle model ages and fractionation factors (Table 4) as well as REE signatures preferably suggest significant contamination by lower continental crust (Fig. 11). The OIB-like geochemical features (Figs. 10C and 10D) suggest that the alkali basalts and andesite were produced in a within-plate setting (Fig. 12A). However, the negative Nb and Ta anomalies of the alkali basalts and andesite were probably produced by slab-derived fluids, hence implying the formation of these rocks in a supra-subduction environment. Therefore, we suggest that a continental back-arc rift could be the most likely tectonic setting for the alkali basalts and andesite which were generated during the very early stages of the opening of the continental back-arc basin.

It is worth to note that the andesite, if compared to the alkali basalts, has

geochemical characteristics closer to OIB (Figs. 10C and 10D). Such OIB-like andesite with a subtle arc signature is analogous to andesites from the Ryukyu arc of SW Japan (Shinjo, 1999) and basaltic andesites in northern Taiwan (Wang et al., 2002). Both were formed in modern back-arc basin settings.

8.2. Lateral correlations of the ophiolitic mélanges in the southern Chinese Tianshan

The geochemical and isotopic features of the Heiyingshan tholeiitic basalts are comparable with those of mafic rocks from adjacent ophiolitic mélange zones. At Wuwamen (Fig. 1B), the source of N-MORB-like tholeiitic basalts was interpreted to have been metasomatized by slab-derived fluids (Dong et al. 2005), and their high primitive-mantle-normalized Th/Nb ratios (1.4-5.9) suggest significant crustal contamination (Saunders et al., 1992). At the Kulehu and Serikeya localities (Fig. 1B), N-MORB-type tholeiite and E-MORB-like alkali basalt were interpreted to be derived from mantle sources with the involvement of sea-floor sediments and the subcontinental lithosphere (Gao et al. 1995a; Tang et al., 1995b; Long et al. 2006; Ma et al. 2006a). The ophiolitic rocks in the Yushugou and Tonghuashan mélanges (Fig. 1C) were also considered to have formed in a back-arc basin (Ma et al., 1990; Shu et al., 2004; Charvet et al., 2007).

The gabbro in the Heiyingshan ophiolite (392 ± 5 Ma) was emplaced contemporaneously with the gabbro and granulite-facies meta-mafic rocks in the Yushugou ophiolite (392-378 Ma; Jiang et al., 2000; Zhou et al., 2004). These ages

are close to that of the basalt from the Kulehu ophiolite (425 Ma; Long et al., 2006). In addition, Late Devonian to early Carboniferous radiolarian-bearing siliceous muddy matrix of the Heiyingshan mélange may be correlated with the Middle Devonian-early Carboniferous radiolarian cherts in the Kulehu and Tonghuashan mélanges (Gao et al., 1998; Liu, 2001; Zhu, 2007).

Structural analyses show that the ophiolitic mélanges in Heiyingshan and adjacent Kulehu, Yushugou and Tonghuashan (Shu et al., 1996; Charvet et al., 2007) tectonically overlie a metamorphosed substratum in which kinematic indicators of top-to-the-north ductile shearing suggest that the ophiolitic mélanges were transported from south to north. Our muscovite $^{40}Ar/^{39}Ar$ dates (359-356 Ma) for mylonitized pelites from the Heiyingshan mélange are consistent with the age of deformation and metamorphism (370-360 Ma) in the Kulehu, Yushugou and Tonghuashan ophiolitic mélanges and their tectonic substrata (Cai et al., 1996; Liu and Qian, 2003; Wang et al., 2003; Li et al., 2004).

In summary, the Heiyingshan ophiolitic mélange is comparable to those in the Kulehu, Serikeya, Wuwamen, Yushugou-Tonghuashan and Aheqi areas in terms of: (1) geochemical affinity and geodynamic setting of mafic rocks; (2) ages of the ophiolitic rocks; (3) timing and kinematics of tectonic emplacement. Therefore, linearly distributed ophiolitic mélange zones in the southern Chinese Tianshan (Fig. 1B) likely represent remnants of a single suture related to the South Tianshan back-arc basin.

Some authors (e.g., Windley et al., 1990; Gao et al., 1998) regarded these

ophiolitic mélange zones as tectonic klippes transported to the south for ca. 100 km from the HP metamorphic belt and the associated ophiolitic mélange zone located farther north (Fig. 1B). Therefore, the HP metamorphic complex and all ophiolitic mélanges within the southern Chinese Tianshan were considered to represent one single suture zone rooted along the Nalati Fault (Fig. 1B). However, this interpretation is not supported by this study and other recent research for the following reasons: (a) kinematic features of the above-mentioned ophiolitic mélange zones (Shu et al., 1996; Charvet et al., 2007; this study) consistently indicate northward emplacement rather than south-verging klippes; (b) T-MORB, OIB and seamounts protoliths of the HP metamorphic rocks and the Xiate-Dalubayi ophiolites show no supra-subduction signature nor continental contamination (Gao et al. 1995b; Qian et al., 2007, 2009; Simonov et al., 2008) and thus have been probably formed in a lager oceanic setting different from the South Tianshan continental back-arc basin; (c) the ages of the mafic rocks in the Xiate-Dalubayi ophiolites (600-516 Ma) are ca. 90-140 Ma older than those of the ophiolitic rocks (425-378 Ma) in Heiyingshan, Kulehu and Yushugou areas; therefore, they most likely belong to a separate (and older) suture zone.

Consequently, at least two suture zones can be distinguished in the southern Chinese Tianshan, namely, a Central Tianshan Suture to the north along the HP metamorphic belt, and a South Tianshan Suture to the south in Heiyingshan-Kulehu, extending eastwards to Wuwamen and Yushugou, and westwards to the Biediele and Aheqi areas (Fig. 1B; Charvet et al., 2007; Wang et al., 2008). The HP metamorphic belt and Xiate ophiolite were also considered to represent two different suture zones

(Qian et al., 2007, 2009; Gao et al., 2009; Charvet et al., in press), but this is beyond the scope of this study.

8.3. An active margin along the northern Tarim craton

The northern Tarim craton has generally been considered as a passive margin characterized by thick Paleozoic carbonate and clastic rocks that are widespread in the south of the Nalati Fault and the MTSZ (Fig. 1B) (e.g., Carroll et al., 1995, 2001; Gao et al., 1998). Nevertheless, several studies during the last decade as summarized below suggested that arc magmatism occurred during the Paleozoic along the northern margin of the Tarim.

Ordovician-Silurian (490-427 Ma) and Early Devonian (~396 Ma) calc-alkaline volcanic and volcaniclastic rocks (Gong et al., 2003; Zhu, 2007) are exposed between the Central Tianshan Suture and the South Tianshan Suture (Fig. 1B). Synchronous arc-type granitoids (447-423 Ma and ~395 Ma) occur between Kulehu and Nalati Pass and also in the Kumux area (Fig. 1B; Xu et al., 2006; Yang and Wang, 2006; Yang et al., 2006). Moreover, in clastic rocks of the Biediele area (Fig. 1B), paleocurrent analysis indicate a derivation from the Tarim for Early Devonian detrital magmatic zircons (Luo et al., 2010). These calc-alkaline igneous rocks and minerals are interpreted to represent an early Paleozoic magmatic arc developed upon a Proterozoic basement and its Neoproterozoic sedimentary cover. The basement rocks represented by Neoproterozoic orthogneiss and pegmatite (Wang et al., 1996; Yang et al., 2006; Zhu and Song, 2006; Zhu, 2007) are similar to those of the Tarim block (Hu

et al., 2000, 2006), but they are separated from the Tarim by the South Tianshan Suture. Thus, this continental magmatic arc, defined as Central Tianshan (Wang et al., 2008), could have been an active margin along the northern Tarim during Ordovician to Silurian times and was rifted from Tarim in late Silurian-Early Devonian due to opening of the South Tianshan back-arc basin.

In the Late Devonian (387-363 Ma), granitoids with calc-alkaline affinity developed in the south of Kulehu and Wuwamen areas (Fig. 1B) (Jiang et al., 2001; Zhu et al., 2008b), and coeval Late Devonian arc-type volcanism occurred in the northern Kuluketage area (Fig. 1B) (Ma et al., 2002). These lines of evidence argue for a Late Devonian magmatic arc to have existed along the northern Tarim craton (Charvet et al., 2007).

8.4. Subduction polarity of the paleo-Tianshan Ocean

In previous tectonic models, a north-directed subduction was proposed for the Paleo-Tianshan Ocean (e.g. Windley et al., 1990; Gao et al., 1998; Chen et al., 1999). In Kyrgyz Tianshan, a north-dipping subduction of Terskey Ocean was also widely accepted (e.g., Mikolaichuk et al., 1997; Konopelko et al., 2008). However, the Terskey Ocean was considered to have been closed in Early Ordovician resulting in a suture zone between the Kyrgyz Central Tianshan and the Kazakhstan-Yili blocks (Mikolaichuk et al., 1997; Burtman, 2006). Eastward extension of this suture zone in China is not clear (Gao et al., 2009) and discussion on this issue is beyond the scope of this study. The suture zone related to the Paleo-Tianshan Ocean (Central Tianshan

Suture) is more likely the eastern extension of the Atbashy-Inylchek zone that probably resulted from closure of the Turkestan Ocean (Burtman, 2006; Biske and Seltmann, 2010). The previously proposed north-dipping subduction was mainly based on (1) south-vergent fold-and-thrust system in the southern Tianshan (e.g., Biske and Seltmann, 2009), (2) arc magmatism in the Yili-Kazakhstan block and in Kyrgyzstan Central Tianshan, and (3) previously considered passive margin along the northern Tarim (e.g., Chen et al., 1999; Carroll et al., 2001).

However, the Paleozoic Tianshan Belt was strongly overprinted by post-orogenic transcurrent and extensional tectonics and Cenozoic intracontinental shortening (Wang et al., 2006, 2009, 2010). As emphasized by Makarov et al. (2010), the state and deep-structure of Paleozoic and older lithotectonic complexes had been changed due to deep denudation and planation before the Cenozoic introcontinental reactivation induced by Indo-Asian collision. Hence, although the post-orogenic wrench faults (e.g., Nikolaev Line) and Cenozoic mega-thrusts may have partially inherited the Paleozoic accretionary structures (Makarov et al., 2010), they cannot be fairly considered to act as a boundary between two continental blocks (Mikolaichuk et al., 1995; Wang et al., 2010). The real plate boundary that was often dislocated by later reactivation could be inferred by occurrence of ophiolitic relics and highly deformed (and metamorphosed) autochthonous substratum, in both of which original structures are preserved to indicate subduction and/or collisional kinematics (Gao et al., 1995; Charvet et al., 2007; Wang et al., 2008, 2010; Lin et al., 2009).

Therefore, south-vergent fold and thrust structures occurring extensively in the

southern Tianshan should be prudently used in reconstructing the subduction polarity of the Paleo-Tianshan Ocean because (i) majority of these structures deformed not only Paleozoic rocks but also Mesozoic-Tertiary rocks showing similar deformation style (imbricate fold-and-thrust belt) (Lu et al., 1994; Allen et al., 1999; Biske and Seltmann, 2010), and are therefore undistinguishable from the Cenozoic structure; (2) some of south-vergent structures could probably be Paleozoic but they re-deformed earlier ductile structures (foliation, lineation and top-to-the-north shear kinematics), and most likely represent back-thrust during a later stage of accretion and collisional orogeny. Taking into account the occurrence of continental arc magmatism in the Chinese Central Tianshan and existence of back-arc basin spreading to the south, a south-directed subduction below the Central Tianshan-northern Tarim seems more favorable for the Paleo-Tianshan Ocean than a northward subduction beneath the Yili-Kazakstan microcontinent. In this case, the arc magmatism in the Chinese Yili-North Tianshan has been considered as a result of south-directed subduction of the North Tianshan oceanic lithosphere (Allen et al., 1993; Charvet et al., 2007; Wang et al., 2008; Han et al., 2010) or, alternatively, as a consequence of bi-directional subduction of the Paleo-Tianshan Ocean (Gao et al., 2009).

However, Paleozoic magmatic rocks and ultramafic-mafic assemblage in the southern Kyrgyz Tianshan (Apayarov et al., 2008) are poorly studied. Thus, westward extension of the Paleozoic active margin along the northern Tarim and back-arc basin-related ophiolitic mélange in Kyrgyzstan remain unclear. Future investigation on age and petrogenesis of these rocks is certainly in need to better understand the

tectonics of the southern Chinese Tianshan in comparing with Kyrgyz sides.

8.5. Paleozoic tectonics of the southern Chinese Tianshan

On the basis of the above discussion, the Chinese Central Tianshan, located between the Central Tianshan Suture and South Tianshan Suture, constituted the northern part of the Tarim craton upon which a magmatic arc developed during the Ordovician to Mid-Silurian. The arc magmatism was probably produced by south-dipping subduction of the Paleo-Tianshan Ocean that separated the Kazakhstan-Yili block to the North from the Central Tianshan-Tarim block to the south (Charvet et al., 2007; Wang et al., 2008; Gao et al., 2009). After a period of active margin magmatism, back-arc extension occurred in the Middle Ordovician-Mid Silurian to produce A-type granites (Han et al., 2004) and OIB-like alkali basalt and andesite (this study) (Fig. 13A). Subsequently, active-margin magmatism temporarily ceased, and a back-arc basin formed since ~425 Ma (Fig. 13B). The opening of the back-arc basin rifted the early Paleozoic Central Tianshan continental arc away from the Tarim block.

In the Middle Devonian, the South Tianshan back-arc basin started to subduct beneath the Tarim block, forming calc-alkaline magmatism along the northern margin of the Tarim (Jiang et al., 2001; Ma et al., 2002; Zhu et al., 2008b) (Fig. 13C). The final closure of the South Tianshan back-arc basin resulted in northward emplacement of the ophiolitic mélanges upon the Central Tianshan. Synchronously, the Paleo-Tianshan Ocean was closed, and the collision between the Kazakhstan-Yili

block and the Central Tianshan-Tarim assemblage occurred during the Late Devonian to early Carboniferous (e.g., Gao and Klemd, 2003; Wang et al., 2010; Fig. 13D).

9. Conclusions

The Heiyingshan mélange of the southern Chinese Tianshan is composed of dismembered ophiolitic rocks and sediments. The petrographic and geochemical data suggest that the gabbro, peridotite and N-MORB-like basalts were derived from depleted mantle, whereas OIB-like basalts and andesite were extensively contaminated by continental crust. The volcanic rocks probably originated in a supra-subduction environment and were variably modified by slab-derived fluids and continental material. The alkali basalts and andesite were produced during back-arc rifting, and tholeiitic basalt, gabbro and peridotite were formed in the South Tianshan back-arc basin initiated along the northern active margin of the Tarim Block.

Our new zircon U-Pb age of the gabbro as well as biostratigraphic data, combined with previously published results, suggest that the South Tianshan back-arc basin formed during the late Silurian to Middle Devonian (425-378 Ma), and existed up to the early Carboniferous (Visean). Field observations, muscovite $^{40}Ar/^{39}Ar$ dating on mylonitic pelites from the mélange, and previously dated arc magmatism all indicate that the back-arc basin began to be subducted in the Middle-Late Devonian and was closed in the early Carboniferous (368-356 Ma). The ophiolitic mélanges were finally emplaced from south to north and thereafter overlain, unconformably, by Serpukhovian-age sediments.

Acknowledgements

We are grateful to Prof. Y.J. Wang (NIGP-CAS) for analysing the radiolarian microfossils, and to Prof. W. Chen (IG-CAGS) for the $^{40}Ar/^{39}Ar$ dating. Mr. F.L. Lin and Mr. W.Y. Hsu of Institute of Earth Sciences-Academia Sinica, and Ms. Y.C. Lin of National Taiwan University, Drs. M.Q. Zhang and T. Yang of Nanjing University are thanked for their assistance in geochemical analyses. Prof. Kröner is appreciated for his help with improving our manuscript. This study was funded by the National Basic Research Program of China (973 Program) (2007CB411301). B.M. Jahn and B. Wang acknowledge financial support of the National Science Council (NSC-Taiwan) through grants numbers: NSC 96-2752-M-002-010-PA, NSC 96-2116-M-001-004, and NSC 97-2752-M-002-003-PA. B. Wang appreciates the support from the Scientific Research Foundation for Returned Overseas Chinese Scholars, State Education Ministry of China. Thanks to reviewers.

REFERENCES CITED

Ai, Y.L., Zhang, L.F., Li, X.P., Qu, J.F., 2006. Geochemical characteristics and tectonic implications of HP-UHP eclogites and blueschists in southwestern Tianshan, China. Progress in Natural Science 16(6), 624-632.

Allen, M.B., Windley, B.F., Zhang, C., 1993. Paleozoic collisional tectonics and magmatism of the Chinese Tien Shan, Central Asia. Tectonophysics 220, 89-115.

Allen, M.B., Vincent, S.J., Wheeler, P.J., 1999. Late Cenozoic tectonics of the Kepingtage thrust zone: interactions of the Tien Shan and Tarim basin, northwest China. Tectonics 1(4), 639–654.

Apayarov, F., Vorob'ev, T., Chernavskaja, Z., Skrinnik, L., Esmintsev, A., Gordeev, D., Ghes, M., 2008. Quaternary removed geological map of the Khan Tengri Massif (1:200,000). Edited by Mikilaichuk, A., Buchroithner, M., Kyrgyz-Russian Slavic University, International Science and Technology Center.

Biske, Y.S., Seltmann, R., 2010. Paleozoic Tian-Shan as a transitional region between the Rheic and Urals-Turkestan oceans. Gondwana Research 17, 602-613.

Bodinier, J.L., Godard, M., 2004. Orogenic, Ophiolitic, and Abyssal Peridotites, in: Carlson, R.W. (Ed.), The Mantle and Core, Treatise on Geochemistry. Oxford, Elsevier-Pergamon 2, pp. 103-170.

Burtman, B.S., 2006. The Tien Shan Early Paleozoic tectonics and geodynamics. Russian Journal of Earth Sciences 8, doi: 10.2205/2006ES000202.

Cai, D.S., Lu, H.F., Jia, D., Wu, S.M., Chen, C.M., 1996. $^{40}Ar/^{39}Ar$ dating of the ophiolite melange in the southern Tien Shan and the mylonite in the southern rim of central Tien Shan and their tectonic significance. Scientia Geologica Sinica 31(4), 384-390 (in Chinese with English

abstract).

Carroll, A.R., Graham, S.A., Chang, E., McKnight, C.L., 2001. Sinian through Permian tectonostratigraphic evolution of the northwestern Tarim basin, China, in: Hendrix, M.S., Davis, G. (Eds.), Paleozoic and Mesozoic tectonic evolution of central and eastern Asia: from continental assembly to intracontinental deformation. Geological Society of America Memoir 194, pp. 47-69.

Carroll, A.R., Graham, S.A., Hendrix, M.S., Ying, D., Zhou, D., 1995. Late Paleozoic tectonic amalgamation of northwestern China: sedimentary record of the north Tarim, northwestern Turpan and southern Junggar basins. Geological Society of America Bulletin 107, 571-594.

Charvet, J., Shu, L.S., Laurent-Charvet, S., 2007. Palaeozoic structural and geodynamic evolution of eastern Tianshan (NW China): welding of the Tarim and Junggar plates. Episodes 30(3), 162-186.

Chen, C.M., Lu, H.F., Jia, D., Cai, D.S., Wu, S.M., 1999. Closing history of the southern Tianshan oceanic basin, western China: an oblique collisional orogeny. Tectonophysics 302, 23-40.

Chen, W., Liu, X.Y., 2002. Continuous laser stepwise heating $^{40}Ar/^{39}Ar$ dating technique. Geological Review 48, 127-134 (in Chinese with English abstract).

Coleman, R.G., 1989. Continental growth of northwest China. Tectonics 8(3), 621-635.

Couture, R.A., Smith, M.S., Dymek, R.F., 1993. X-ray fluorescence analysis of silicate rocks using fused glass discs and a side-window Rh source tube: accuracy, precision and reproducibility. Chemical Geology 110, 315-328.

Dobretsov, N.L., Coleman, R.G., Liou, J.G., Maruyama, S., 1987. Blueschist belt in Asia and possible periodicity of blueschist facies metamorphism. Ofioliti 12, 445-456.

Dong, Y.P., Zhou, D.W., Zhang, G.W., Zhang, C.L., Xia, L.Q., Xu, X.Y., Li, X.M., 2005. Tectonic setting of the Wuwamen ophiolite at the southern margin of Middle Tianshan Belt. Acta Petrologica Sinica 21(1), 37-44 (in Chinese with English abstract).

Dong, Y.P., Zhou, D.W., Zhang, G.W., Zhao, X., Luo, J.H., Xu, J.G., 2006. Geology and geochemistry of the Gangou ophiolitic mélange at the northern margin of the Middle Tianshan Belt. Acta Petrologica Sinica 22(1), 49-56 (in Chinese with English abstract).

Gao, J., Klemd, R., 2003. Formation of HP-LT rocks and their tectonic implications in the western Tianshan Orogen, NW China: geochemical and age constraints. Lithos 66, 1-22.

Gao, J., He, G.Q., Li, M.S., Xiao, X.C., Tang, Y.Q., 1995b. The mineralogy, petrology, metamorphic PTDt trajectory and exhumation mechanism of blueschists, south Tianshan, northwestern China. Tectonophysics 250, 151-168.

Gao, J., Klemd, R., Zhang, L.F., Wang, Z., Xiao, X.C., 1999. P–T path of high pressure–low temperature rocks and tectonic implications in the western Tianshan Mountains (NW China). Journal of Metamorphic Geology 17, 621–636.

Gao, J., Li, M.S., Xiao, X.C., Tang, Y.Q., He, G.Q., 1998. Paleozoic tectonic evolution of the Tianshan Orogen, northern China. Tectonophysics 287, 213-231.

Gao, J., Long, L.L., Klemd, R., Qian, Q., Liu, D.Y., Xiong, X.M., Su, W., Liu, W., Wang, Y.T., Yang, F.Q., 2009. Tectonic evolution of the South Tianshan orogen and adjacent regions, NW China: geochemical and age constraints of granitoid rocks. International Journal of Earth Sciences 98, 1221-1238.

Gao, J., Long, L.L., Qian, Q., Huang, D.Z., Su, W., Klemd, R., 2006. South Tianshan: a Late Paleozoic or a Triassic orogen? Acta Petrologica Sinica 22(5), 1049-1061 (in Chinese with English

abstract).

Gao, J., Tang, Y.Q., Zhao, M., Wang, J., 1995a. The formation environment of ophiolites in Haerk Mountains, Xinjiang. Earth Sciecens 20(6), 682-688 (in Chinese with English abstract).

Gao, J., Xiao, X.C., Tang, Y.Q., Zhao, M., Wang, J., Wu, H.Q., 1993. The discovery of blueschist in Kumux of the southern Tien Shan and its tectonic significance. Regional Geology of China 4, 344-347 (in Chinese with English abstract).

Gao, J., Zhang, L.F., Liu, S.W., 2000. The $^{40}Ar/^{39}Ar$ age record of formation and uplift of the blueschists and eclogites in the western Tianshan Mountains. Chinese Science Bulletin 45, 1047–1051.

Gao, J.F., Lu, J.J., Lai, M.Y., Lin, Y.P., Pu, W., 2003. Analysis of trace elements in rock samples using HR-ICPMS. Journal of Nanjing University (Natural Sciences) 39(6), 844-850 (in Chinese with English abstract).

Gong, F.H., Li, Y.J., Wang, Q.H., Hu, S.L., Huang, Z.B., Luo, J.C., 2003. New Ar-Ar geochronologic data of Paleozoic volcanic rocks in the western segment of Chinese Southern Tianshan. Geological Journal of China Universities 9(3), 494-498 (in Chinese with English abstract).

Han, B.F., He, G.Q., Wu, T.R., Li, H.M., 2004. Zircon U-Pb dating and geochemical features of Early Paleozoic granites from Tianshan, Xinjiang: Implications for tectonic evolution. Xinjiang Geology 22(1), 4-11 (in Chinese with English abstract).

Hawkins, J.W., 2003. Geology of supra-subduction zones-Implications for the origin of ophiolites, in: Dilek, Y., Newcomb, S. (Eds.), Ophiolite concept and the evolution of geological thought. Geological Society of America Special Paper 373, pp. 227-268.

Hendrix, M.S., Dumitru, T.A., Graham, S.A., 1994. Late Oligocene-Early Miocene unroofing in the

Chinese Tian Shan: An early effect of the India-Asia collision. Geology 22, 487-490.

Hopson, C., Wen, J., Tilton, G., Tang, Y., Zhu, B., Zhao, M., 1989. Paleozoic plutonism in East Junggar, Bogdashan, and eastern Tianshan, NW China. EOS (Transactions, American Geophysical Union) 70, 1403–1404.

Hu, A.Q., Jahn, B.M., Zhang, G.X., Zhang, Q.F., 2000. Crustal evolution and Phanerozoic crustal growth in Northern Xinjiang: Nd-Sr isotopic evidence. Part I: Isotopic characterization of basement rocks. Tectonophysics 328, 15-51.

Hu, A.Q., Zhang, G.X., Chen, Y.B., 2006. Isotope geochronology and geochemistry for major geological events of continental crustal evolution of Xinjiang, China. Geological Publishing House, Beijing (in Chinese with English abstract).

Jahn, B.M., 2004. The Central Asia Orogenic Belt and growth of the continental crust in the Phanerozoic, in: Malpas, J., Fletcher, C.J.N., Ali, J.R., Aitchison, J.C. (Eds.), Aspects of the tectonic evolution of China. Geological Society of London Special Publication 226, pp. 73-100.

Jahn, B.M., Bernard-Griffiths, J., Charlot, R., Cornichet, J., Vidal, F., 1980. Nd and Sr isotopic compositions and REE abundances of Cretaceous MORB (Holes 417D and 418A, Legs 51, 52 and 53). Earth and Planetary Science Letters 48, 171-184.

Jahn, B.M., Griffin, W.L., Windley, B.F., 2000. Continental growth in the Phanerozoic: evidence from Central Asia. Tectonophysics 328, 1-227.

Jahn, B.M., Litvinovsky, B., Zanvilevich, A.N., Reichow, M., 2009. Peralkaline granitoid magmatism in the Mongolian-Transbaikalian Belt: evolution, petrogenesis and tectonic significance. Lithos 113, 521-539.

Jiang, C.Y., Li, L.C., 1990. Petrology and geochemistry of layered cumulation rocks in Yushugou,

Xinjiang. Minerals and Rocks 10(2), 31-36 (in Chinese with English abstract).

Jiang, C.Y., Mu, Y.M., Zhao, X.N., Zhang, H.B., 2000. The geological features and tectonic significance of a mafic-ultramafic complex belt at the northern margin of the southern Tien Shan fold belt, China. Journal of Xi'an Engineering University 22(2), 1-6 (in Chinese with English abstract).

Jiang, C.Y., Mu, Y.M., Zhao, X.N., Bai, K.Y., Zhang, H.B., 2001. Petrology and geochemistry of active continental margin intrusive rock belt on the northern margin of the Tarim. Regional Geology of China 20(2), 158-163 (in Chinese with English abstract).

Khain, E.V., Bibikova, E.V., Salnikova, E.E., Kröner, A., Gibsher, A.S., Dddenko, A.N., Egtyarev, K.E., Fdotova, A.A., 2003. The Palaeo-Asian ocean in the Proterozoic and early Palaeozoic: new geochronologic data and palaeotectonic reconstructions. Precambrian Research 122, 329-358.

Kim, J., Coish, R., Evans, M., Dick, G., 2003. Supra–subduction zone extensional magmatism in Vermont and adjacent Quebec: Implications for early Paleozoic Appalachian tectonics. Geological Society of America Bulletin 115, 1552-1569.

Klemd, R., Bröcker, M., Hacker, B.R., Gao, J., Gans, P., Wemmer, K., 2005. New age constraints on the metamorphic evolution of the high-pressure/low-temperature belt in the western Tianshan mountains, NW China. Journal of Geology 113, 157–168.

Konopelko, D., Biske, G., Seltmann, R., Kiseleva, M., Matukov, D., Sergeev, S., 2008. Deciphering Caledonian events: Timing and geochemistry of the Caledonian magmatic arc in the Kyrgyz Tien Shan. Journal of Asian Earth Sciences 32, 131–141.

Kröner, A., Windley, B.F., Badarch, G., Tomurtogoo, O., Hegner, E., Jahn, B.M., Gruschka, S., Khain, E.V., Demoux, A., Wingate, M.T.D., 2007. Accretionary growth and crust-formation in the

Central Asian Orogenic Belt and comparison with the Arabian-Nubian Shield, in: Hatcher, R.D.Jr., Carlson, M.P., McBride, J.H., Catalan, J.M. (Eds.), 4-D framework of the continental crust-Integrating crustal processes through time. Geological Society of America Memoir 200, pp. 181-209.

Laurent-Charvet, S., 2001. Accrétions continentales en Asie centro-orientale: évolution géodynamique et structurale du Tianshan et du Junggar oriental (nord-ouest Chine) au Paléozoïque. PhD thesis, University of Orléans, Orléans, France.

Li, X.D., Xiao, W.J. Zhou, Z.L., 2004. $^{40}Ar/^{39}A$ age determination on the Late Devonian tectonic event along the southern margin of the South Tianshan Mountains and its significance. Acta Geologica Sinica 20(3), 691-696 (in Chinese with English abstract).

Lin, W., Faure, M., Shi, Y.H., Wang, Q.C., Li, Z., 2009. Palaeozoic tectonics of the south-western Chinese Tianshan: new insights from a structural study of the high-pressure/low-temperature metamorphic belt. International Journal of Earth Sciences 98, 1259-1274.

Liou, J.G., Graham, S.A., Maruyama, S., Zhang, R., 1996. Characteristics and tectonic significance of the Late Proterozoic Aksu blueschists and diabasic dikes, Northwest Xinjiang, China. International Geological Review 38, 228- 244.

Liu, B., Qian, Y.X., 2003. The geologic characteristics and fluid evolution in the three high-pressure metamorphic belts of eastern Tianshan. Acta Petrologica Sinica 19(2), 283-296 (in Chinese with English abstract).

Liu, C.X., Xu, B.L., Zou, T.R., Lu, F.X., Tong, Y., Cai, J.H., 2004. Petrochemistry and tectonic significance of Hercynian alkaline rocks along the northern margin of the Tarim platform and its adjacent area. Xinjiang Geology 22(1), 43-49 (in Chinese with English abstract).

Liu, Y., 2001. Early Carboniferous radiolarian fauna from Heiyingshan, South of the Tianshan Mountains and its geotectonic significance. Acta Geologica Sinica 75(1), 101-108.

Liu, Z.R., Pei, J.P., Deng, D.S., Sun, J.H., Tao, L., 2005. Ordovician ophiolite in Xin'Gangou of Tuokexun, Xinjiang. Xinjiang Geology 23(4), 326-333 (in Chinese with English abstract).

Long, L.L., Gao, J., Xiong, X.M., Qian, Q., 2006. The geochemical characteristics and the age of the Kule Lake ophiolite in the southern Tianshan. Acta Petrologica Sinica 22(1), 65-73 (in Chinese with English abstract).

Lu, H.F., Howell, D.C., Jia, D., 1994. Rejuvenation of the Kuqa foreland basin, northern flank of the Tarim basin, Northwest China. International Geological Review 36, 1151-1158.

Lu, S.N., Li, H.K., Zhang, C.L., Niu, G.H., 2008. Geological and geochronological evidence for the Precambrian evolution of the Tarim Craton and surrounding continental fragments. Precambrian Research 160, 94-107.

Luo, Y.J., Wang, G.C., Cao, S.Z., Gao, R., Liu, H., Huang, W.X., 2010. Provenance and tectonic implication of detrital zircons in Silurian-Devonian clastic rocks from basin-rang linking areas, NW Tarim, in: Proceedings of the 3rd National Symposium on Structural Geology and Geodynamics, Guangzhou (China), pp. 155 (in Chinese).

Ma, H.F., Zhang, Z.M., Cai, G.Q., Li, Y.X., 2002. Zonation characteristics of gold mineralization in eastern part of southern Tianshan and prospect prognosis. Uranium Geology 18, 282-286 (in Chinese with English abstract).

Ma, R.S., Ye, S.F., Wang, C.Y. Liu, G.B., 1990. Framework and evolution in the East Tianshan Orogenic belt. Geosciences of Xinjiang 2, 21-36 (in Chinese with English abstract).

Ma, Z.P., Xia, L.Q., Xu, X.Y., Li, X.M., Xia, Z.C., Wang, L.S., 2006b. The tectonic setting and implication of volcanic-magmatic complex from the Upper-Silurian Bayinbuluke Formation, Southern Tianshan. Journal of Jilin University (Earth Science Edition) 36(5), 736-743 (in

Chinese with English abstract).

Ma, Z.P., Xia, L.Q., Xu, X.Y., Xia, Z.C., Li, X.M., Wang, L.S., 2006a. Geochemical characteristics of basalts: evidence for the tectonic setting and geological significance of Kulehu ophiolite, South Tianshan Mountains. Acta Petrologica et Mineralogica 25(5), 387-400 (in Chinese with English abstract).

Makarov, V.I., Alekseev, D.V., Batalev V.Y., Bataleva, E.A., Belyaev, I.V., Bragin, V.D., Dergunov, N.T., Efimova, N.N., Leonov, M.G., Munirova, L.M., Pavlenkin, A.D., Roecker, S., Roslov, Y.V., Rybin, A.K., Shchelochkov, G.G., 2010. Underthrusting of Tarim beneath the Tien Shan and Deep structure of their junction zone: Main results of seismic experiment along MANAS profile Kashgar-Song-Köl. Geotectonics (English translation) 44(2), 102-126.

Meschede, M., 1986. A method of discriminating between different types of mid-ocean ridge basalts and continental tholeiites with the Nb-Zr-Y diagram. Chemical Geology 56, 207-218.

Metcalf, R.V. Shervais, J.W., 2008. Supra-subduction zone ophiolites: Is there really an ophiolite conundrum? in: Wright, J.E., Shervais, J.W. (Eds.), Ophiolites, Arcs, and Batholiths. Geological Society of America Special Paper 438, pp. 191-222.

Mikolaichuk, A.V., Kotov, V.V., Kuzikov, S.I., 1995. Structural position of the Malyi Naryn metamorphic complex as related to the problem of the boundary between the North and Median Tian Shan. Geotectonics (English translation) 29(2), 157-166.

Mikolaichuk, A.V., Kurenkov, S.A., Degtyarev, K.E., Rubtsov, V.I., 1997. Northern Tien Shan: Main stages of geodynamic evolution in the late Precambrian-early Paleozoic. Geotectonics (English translation) 31(6), 445-462.

Qian, Q., Gao, J., Klemd, R., He, G.Q., Song, B., Liu, D.Y., Xu, R.H., 2008. Early Paleozoic tectonic

evolution of the Chinese South Tianshan Orogen: constraints from SHRIMP zircon U–Pb geochronology and geochemistry of basaltic and dioritic rocks from Xiate, NW China. International Journal of Earth Sciences 98, 551-569.

Qian, Q., Xu, S.L., He, G.Q., Klemd, R., Xiong, X.M., Long, L.L., Gao, J., 2007. Elemental geochemistry and tectonic significance of Cambrian basalts from the northern side of the Nalati Mountain. Acta Petrologica Sinica 23, 1708-1720 (in Chinese with English abstract).

Rollinson, H.R., 1993. Using Geochemical Data: evaluation, presentation, interpretation. Longman scientific technical, New York.

Saunders, A.D., Storey, M., Kent, R.W., Norry, M.J., 1992. Consequences of plume lithosphere interactions, in: Storey, B.C. (Ed.), Magmatism and the Causes of Continental Break-up. Geological Society of London Special Publications 68, pp. 41-60.

Sengör, A.M.C., Natal'in, B.A., 1996. Paleotectonics of Asia: fragments of a synthesis, in: Yin, A., Harrison, M. (Eds.), The Tectonic Evolution of Asia. Rubey Colloquium. Cambridge University Press, Cambridge, pp. 486–640.

Sengör, A.M.C., Natal'in, B.A., Burtman, V.S., 1993. Evolution of the Altaid tectonic collage and Paleozoic crust growth in Eurasia. Nature 364, 299–307.

Shi, Y.R., Liu, D.Y., Zhang, Q., Jian, P., Zhang, F.Q., Miao, L.C., 2007. SHRIMP zircon U-Pb dating of the Gangou granitoids, Central Tianshan Mountains, Northwest China and tectonic significances. Chinese Science Bulletin 52, 1507-1516.

Shinjo, R., 1999. Geochemistry of high Mg andesites and the tectonic evolution of the Okinawa Trough–Ryukyu arc system. Chemical Geology 157, 69-88.

Shu, L.S., Charvet, J., Lu, H.F., Laurent-Charvet, S., 2002. Paleozoic accretion-collision events and

kinematics of ductile deformation in the central-southern Tianshan Belt, China. Acta Geologica Sinica 76(3), 308-323.

Shu, L.S., Wang, B., Zhu, W.B., 2007. Age and tectonic significance of radiolarian fossils from the Heiyingshan ophiolitic melange, South Tianshan Belt, NW China. Acta Geologica Sinica 81, 1-8 (in Chinese with English abstract).

Shu, L.S., Wang, C.Y., Ma, R.S., 1996. Granulite relics and pyroxene-facies ductile deformation in the northern boundary of the southern Tianshan. Scientia Geologica Sinica 31(4), 63–71 (in Chinese with English abstract).

Shu, L.S., Yu, J.H., Charvet, J., Laurent-Charvet, S., Sang, H.P., Zhang, R.G., 2004. Geological, geochronological and geochemical features of granulites in the Eastern Tianshan, NW China. Journal of Asian Earth Sciences 24(1), 25-41.

Simonov, V.A., Sakiev, K.S., Volkova, N.I., Stupakov, S.I., Travin, A.V., 2008. Conditions of formation of the Atbashi Ridge eclogites (South Tien Shan). Russian Geology and Geophysics 49, 803–815.

Stupakov, S.I., Volkova, N.I., Travin, A.V., Simonov, V.A., Sakiev, K.S., Novgorodtsev, O.S., 2004. Eclogites of Atbashi Ridge as indicators of Early Carboniferous collision in southern Tien Shan. Petrology of magmatic and metamorphic complexes 4, Tomsk Center for Scientific and Technical Information, Tomsk, pp. 272–277.

Sun, S.S., McDonough, W.F., 1989. Chemical and isotopic systematics of ocean island basalts: implications for mantle composition and processes, in: Saunders, A.D., Norry, M.J. (Eds.), Magmatism in the Ocean Basins. Geological Society of London Special Publications 42, pp. 313-345.

Tang, Y.Q., Gao, J., Zhao, M., Li, J.Y., Wang, J., 1995. The ophiolites and blueschists in the Southwestern Tianshan orogenic belt, Xinjiang, Northwestern China. Geological Publishing House, Beijing (in Chinese with English abstract).

Vavra, G., Gebauer, D., Schmid, R., Compston, W., 1996. Multiple zircon growth and recrystallization during polyphase Late Carboniferous to Triassic metamorphism in granulites of the Ivrea Zone (Southern Alps): an ion microprobe (SHRIMP) study. Contributions to Mineralogy and Petrology 122, 337-358.

Wang, B., Cluzel, D., Shu, L.S., Faure, M., Charvet, J., Chen, Y., Meffre, S., de Jong, K., 2009. Evolution of calc-alkaline to alkaline magmatism through Carboniferous convergence to Permian transcurrent tectonics, western Chinese Tianshan. International Journal of Earth Sciences 98(6), 1275-1298.

Wang, B., Faure, M., Cluzel, D., Shu, L.S., Charvet, J., Meffre, S., 2006. Late Paleozoic tectonic evolution of the northern West Tianshan, NW China. Geodinamica Acta 19(3-4), 237-247.

Wang, B., Faure, M., Shu, L.S., Cluzel, D., Charvet, J., de Jong, K., Chen, Y., 2008. Paleozoic geodynamic evolution of the Yili Block, Western Chinese Tianshan. Bulletin de la Société Géologique de France 179(5), 483-490.

Wang, B., Faure, M., Shu, L.S., de Jong, K., Charvet, J., Cluzel, D., Jahn, B.M., Chen, Y., Ruffet, G., 2010. Structural and geochronological study of High-Pressure metamorphic rocks in the Kekesu section (Northwestern China): implications for the late Paleozoic tectonics of the southern Tainshan. Journal of Geology 118, 59-77.

Wang, B., Shu, L.S., Cluzel, D., Faure, M., Charvet, J., 2007a. Geochemical Constraints on Carboniferous Volcanic rocks of Yili Block (Xinjiang, NW China); implication on tectonic

evolution of Western Tianshan. Journal of Asian Earth Sciences 29, 148-159.

Wang, B., Shu, L.S., Faure, M., Cluzel D., Charvet, J., 2007b. Paleozoic tectonism and magmatism of Kekesu-Qiongkushitai section in southwestern Chinese Tianshan and their constraints on the age of the orogeny. Acta Petrologica Sinica 23(6), 1354-1368 (in Chinese with English abstract).

Wang, B.Y., Li, Q., Liu, J.B., 1997. Geological structures of the Middle Tianshan Mountains along the Dushanzi-Kuqa highway. Xinjiang Geology 15(2), 135-154 (in Chinese with English abstract).

Wang, K.L., Chung, S.L., Chen, C.H., Chen, C.H., 2002. Geochemical constraints on the petrogenesis of high-Mg basaltic andesites from the Northern Taiwan Volcanic Zone. Chemical Geology 182, 513-528.

Wang, R.S., Zhou, D.W., Wang, Y., Wang, J.L., Sang, H.Q., Zhang, R.H., 2003. Geochronology for the multi-stage metamorphism of high-pressure terrain of granulite facies from Yushugou area, south Tianshan. Acta Petrologica Sinica 19(3), 452-460 (in Chinese with English abstract).

Wang, X.C., He, G.Q., Gao, J., Li, M.S., Lu, S.N., 1995a. Structural reformation and age of metamorphic rock series in Lake Kule of souther Tianshan. Xinjiang Geology 13(3), 241-250 (in Chinese with English abstract).

Wang, X.C., He, G.Q., Li, M.S., 1996. A discussion on the time of the Kuergan micro-massif in South Tianshan. Journal of Chengdu University of Technology 23(3), 90-95 (in Chinese with English abstract).

Wang, X.C., He, G.Q., Li, M.S., Gao, J., Lu, S.N., 1995b. Petrochemical characteristics and isotopic age of ophiolite in southern part of south Tianshan. Journal of Hebei College of Geology 18(4), 295-302 (in Chinese with English abstract).

Wilson, M., 1989. Igneous Petrogenesis. Unwin Hyman, London.

Winchester, J.A., Floyd, P.A., 1976. Geochemical magma type discrimination: application to altered and metamorphosed basic igneous rocks. Earth and Planetary Science Letters 28, 459-469.

Winchester, J.A., Floyd, P.A., 1977. Geochemical discrimination of different magma series and their differentiation products using immobile elements. Chemical Geology 20, 325-343.

Windley, B.F., Alexeiev, D., Xiao, W.J., Kroner, A., Badarch, G., 2007. Tectonic models for accretion of the Central Asian Orogenic Belt. Journal of the Geological Society 164, 31-47.

Windley, B.F., Allen, M.B., Zhang, C., Zhao, Z.Y., Wang, G.R., 1990. Paleozoic accretion and Cenozoic redeformation of the Chinese Tien Shan range, Central Asia. Geology 18, 128-131.

Woodhead, J., Eggins, S., Gamble, J., 1993. High field strength and transition element systematics in island arc and back-arc basin basalts: evidence for multiphase extraction and a depleted mantle wedge. Earth and Planetary Science Letters 114, 491-504.

XBGMR (Xinjiang Bureau of Geology and Mineral Resources), 1993. Regional geology of Xinjiang Uygur Autonomy Region. Geological Publishing House, Beijing (in Chinese with English abstract).

XBGMR, 1983. geological map 1:20 0000, Heiyingshan sheet (K-44-10).

Xiao, W.J., Huang, B.C., Han, C.M., Sun, S., Li, J.L., 2010. A review of the western part of the Altaids: A key to understanding the architecture of accretionary orogens. Gondwana Research, doi: 10.1016/j.gr.2010.01.007.

Xiao, W.J., Zhang, L.C., Qin, K.Z., Sun, S., Li, J.L., 2004. Paleozoic accretionary and collisional tectonics of the eastern Tianshan (China): implications for the continental growth of Central Asia. American Journal of Science 304, 370-395.

Xiao, X.C., Tang, Y.Q., Feng, Y.M., Zhu, B.Q., Li, J.Y., Zhao, M., 1992. Tectonic evolution of the

northern Xinjiang and its adjacent regions. Geology Publishing House, Beijing (in Chinese with English abstract).

Xiao, X.C., Tang, Y.Q., Li, J.Y., Zhao, M., Feng, Y.M., Zhu, B.Q., 1990. Geotectonic evolution of northern Xinjiang. Geoscience Xinjiang 1, 47-68.

Xu, X.Y., Ma, Z.P., Li, X.M., He, S.P., Yang, J.L., 2003. The discovery of P-MORB in Jigen area of southwest Tianshan Mountains and its tectonic implications. Acta Petrologica et Mineralogica 22(3), 245-253 (in Chinese with English abstract).

Xu, X.Y., Ma, Z.P., Xia, Z.C., Xia, L.Q., Li, X.M., Wang, L.S., 2006. TIMS U-Pb isotopic dating and geochemical characteristics of Paleozoic granitic rocks from the Middle-Western section of Tianshan. Northwestern Geology 39(1), 50-75 (in Chinese with English abstract).

Yang, H.B., Gao, P., Li, B., Zhang, Q.J., 2005a. The geological character of the Sinian Dalubayi ophiolite in the west Tianshan, Xinjiang. Xinjiang Geology 23(2), 123-126 (in Chinese with English abstract).

Yang, J.H., Chung, S.L., Wilde S.A., Wu F.Y., Chu M.F., Lo C.H., Fan H.R., 2005b. Petrogenesis of post-orogenic syenites in the Sulu Orogenic Belt, East China: geochronological, geochemical and Nd–Sr isotopic evidence. Chemical Geology 214, 99-125.

Yang, S.H., Zhou, M.F., 2009. Geochemistry of the ~430-Ma Jingbulake mafic–ultramafic intrusion in Western Xinjiang, NW China: Implications for subduction related magmatism in the South Tianshan orogenic belt. Lithos 113, 259-273.

Yang, T.N., Wang, X.P., 2006. Geochronology, petrochemistry and tectonic implications of Early Devonian plutons in Kumux area, Xinjiang. Acta Petrologica et Mineralogica 25(5), 401-411 (in Chinese with English abstract).

Yang, T.N., Li, J.Y., Sun, G.H., Wang, Y.B., 2006. Earlier Devonian active continental arc in Central Tianshan: evidence of geochemical analyses and Zircon SHRIMP dating on mylonitized granitic rock. Acta Geologica Sinica 22(1), 41-48 (in Chinese with English abstract).

Zhang, L.C., Wu, N.Y., 1985. Tectonics and evolution of the Tianshan Mountains. Xinjing Geology 3(3), 1-14 (in Chinese with English abstract).

Zhou, D., Graham, S.A., Chang, E.Z., Wang, B.Y., Hacker B., 2001. Paleozoic tectonic amalgamation of the Chinese Tianshan: Evidence from a transect along the Dushanzi-Kuqa highway, in: Hendrix, M.S., Davis, G.A. (Eds.), Paleozoic and Mesozoic tectonic evolution of central Asia: from continental assembly to intracontinental deformation. Geological Society of America Memoir, Boulder, Colorado, 194, pp. 23-46.

Zhou, D.W., Su, L., Jian, P., Wang, R.S., Liu, X.M., Lu, G.X., Wang, J.L., 2004. Zircon U-Pb SHRIMP ages of Yushugou ophiolitic terrane in Southern Tianshan and their tectonic implications. Chinese Science Bulletin 49(13), 1415-1419.

Zhu, Y.F., Song, B., 2006. Petrology and SHRIMP chronology mylonitized Tianger granite, Xinjiang, also about the dating on hydrothermal zircon rim in granite. Acta Petrologica Sinica 22(1), 135-144 (in Chinese with English abstract).

Zhu, Y.F., Zhang, L.F., Gu, L.B., Guo, X., Zhou, J., 2005. The zircon SHRIMP chronology and trace element geochemistry of the Carboniferous volcanic rocks in western Tianshan Mountains. Chinese Science Bulletin 50(19), 2201-2212.

Zhu, Y.F., Zhou, J., Guo, X., 2006a. Petrology and Sr-Nd isotopic geochemistry of the Carboniferous volcanic rocks in the western Tianshan Mountains, NW China. Acta Petrologica Sinica 22(5), 1341-1350 (in Chinese with English abstract).

Zhu, Y.F., Zhou, J., Song, B., Zhang, L.F., Guo, X., 2006b. Age of the "Dahalajunshan" Formation in Xinjiang and its disintegration. Geology in China 33(3), 487-497 (in Chinese with English abstract).

Zhu, Z.X., 2007. The Geological components and tectonic evolution of south Tianshan, Xinjiang. PhD thesis, Chinese Academy of Geological Sciences, Beijing.

Zhu, Z.X., Li, J.Y., Dong, L.H., Wang, K.Z., Liu, G.Z., Li, Y.P., Liu, Z.T., 2008b. Age determination and geological significance of Devonian granitic intrusions in Seriyakeyilake region, northern margin of Tarim basin, Xinjiang. Acta Petrologica Sinica 24, 971-976 (in Chinese with English abstract).

Zhu, Z.X., Li, J.Y., Dong, L.H., Zhang, X.F., Hu, J.W., Wang, K.Z., 2008a. The age determination of Late Carboniferous intrusions in Mangqisu region and its constraints to the closure of oceanic basin in South Tianshan, Xinjing. Acta Petrologica Sinica 24, 2761-2766 (in Chinese with English abstract).

Zhu, Z.X., Wang, K.Z., Zheng, Y.J., Sun, G.H., Zhang, C., Li, Y.P., 2006c. Zircon SHRIMP dating of Silurian and Devonian granitic intrusions in the southern Yili block, Xinjiang and preliminary discussion on their tectonic setting. Acta Petrologica Sinica 22, 1193-1200 (in Chinese with English abstract).

Zindler, A., Hart, S., 1986. Chemical geodynamics. Annual Review of Earth and Planetary Sciences 14, 493-571.

Figure and Table captions

Fig. 1. (A) Sketch map of eastern Eurasia (modified from Jahn, 2004), showing the location of the study area. CAOB = Central Asian Orogenic Belt; EEC = East European Craton; KZN = Kazakhstan; QQ = Qaidam Qinling. (B) Geological map of the western Chinese Tianshan Belt (modified from XBGMR, 1993). Numbers 1 and 2 correspond to the Nalati Fault and the Main Tianshan Shear Zone (MTSZ), respectively. Letters refer to localities cited in the text, a-Aheqi, b-Biediele, c-Changawuzi, d-Dalubayi, g-Gangou, h-Heiyingshan, k-Kulehu, m-Mishigou, n-Nalati, w-Wuwamen, s-Serikeya, t-Tonghuashan, x-Xiate, and y-Yushugou. (C) Topographic image of the Tianshan Mountains and adjacent sedimentary basins, indicating location of the Nalati Fault (1), MTSZ (2) and the Heiyingshan ophiolitic mélange (black pentacle stars).

Fig. 2. (A) Structural map of the Heiyingshan area, SW Chinese Tianshan (modified after XBGMR, 1983), the location is shown in Fig. 1B. The inset shows lower hemisphere Schmidt plots of planar and linear elements observed in the Heiyingshan mélange. (B) Cross-section of the Heiyingshan ophiolitic mélange showing its present contact with Early Paleozoic metamorphic rocks and the Late Paleozoic nonmetamorphic series, a pre-Permian top-to-the-north thrust of the mélange unit is also proposed.

Fig. 3. Field photographs of the Heiyingshan ophiolitic mélange: (A) pillow lava, (B)

sheeted diabase (dike) surrounded by the serpentinized peridotite, (C) sheared serpentinite with calcite veins, (D) limestone ("L") olistoliths, (E) pebbly mudstone, (F) folded calcareous turbidite with disrupted beds corresponding to the matrix of the mélange, (G) blocks of chert and limestone ("L") included in the sheared muddy matrix, fibrous quartz or calcite pressure shadows crystallized around sigmoid limestone clasts indicating top-to-the north sense of shear, (H) Devonian foliated marble corresponding to the tectonic substratum (i.e. autochthonous lower unit) underlying the mélange; the flat slaty cleavage dips to the northwest.

Fig. 4. Field and microphotographs of deformation in the Southern Tianshan mélanges and autochthonous substratum: (A) matrix of the Kulehu mélange with sigmoid volcanic clasts and shear bands indicating top-to-the north shearing; (B) intra-folial asymmetric folds showing top-to-the-north sense of shear and reworked by south-directed thrusting; (C) Devonian mylonitic marble of Biediele valley (Fig. 1B for location); (D-E) microphotographs of foliated volcanic and clastic rocks located below the marble series of the Biediele area, along the N-S trending lineation where drag folds (D) and pressure shadow around pyrite (E) show top-to-the-north shearing; (F) asymmetrically sheared layers in metapelite below the Yushugou ophiolitic mélange showing top-to-the-north shearing.

Fig. 5. Tera-Wasserburg concordia diagram of LA-ICPMS U-Pb isotopic data of

zircons from a gabbro block in the Heiyingshan ophiolitic mélange. Inset shows distribution of the apparent $^{206}Pb/^{238}U$ ages.

Fig. 6. $^{40}Ar/^{39}Ar$ age spectra of muscovites from mylonitic matrix of the Heiyingshan mélange.

Fig. 7. Scanning electron microscope pictures of representative radiolarian microfossils obtained from the siliceous muddy matrix of the Heiyingshan mélange. Fossils Nos. 2, 3 and 27 were obtained from samples 512 and 512-1; Nos. 12 and 15 are from sample 508; and No. 20 is from sample 510. Scale bars correspond to 100 μm.

Fig. 8. Photomicrographs of magmatic rocks from the Heiyingshan mélange: (A) dunite showing serpentinized (srp) olivine (ol) and vermicular spinels (spl), (B) coarse-grained gabbro with cumulate texture made up of inter-growing plagioclase (pl), clinopyroxene (cpx) and amphibole (amp) (C) porphyritic basalt with plagioclase phenocrysts, (D) fine-grained basalt including feldspar (fds), pyroxene (py) and Fe-Ti oxide (ox).

Fig. 9. Classification diagrams for volcanic rocks from the Heiyingshan ophiolitic mélange: (A) Zr/TiO_2 vs. Nb/Y diagram after Winchester and Floyd (1977), (B) TiO_2 vs. $Zr/P_2O_5 \times 10000$ diagram after Winchester and Floyd (1976).

Fig. 10. Chondrite-normalized REE patterns and Primitive Mantle-normalized multi-element diagrams for tholeiitic basalts (A and B) and alkali basalts (C and D) in the Heiyingshan mélange. Normalization values are after Sun and McDonough (1989).

Fig. 11. $\varepsilon_{Nd}(t)$ vs. $I_{Sr}(t)$ diagram for volcanic rocks of the Heiyingshan ophiolitic mélange, T (395 Ma) is the age of the volcanic rocks supposed to be contemporaneous with the dated gabbro. Reference fields for MORB and OIB are after Zindler and Hart (1986).

Fig. 12. Discrimination diagrams for the tectonic setting of magmatic rocks from the Heiyingshan ophiolitic mélange: (A) Zr/4-Nb×2-Y diagram after Meschede (1986), (B) Th/Yb vs. Nb/Yb diagram after Metcalf and Shervais (2008).

Fig. 13. Simplified tectonic model for the Paleozoic evolution of the southern Chinese Tianshan (modified from Wang et al., 2008) (see discussion for details).

Table 1. Zircon U-Pb LA-ICPMS analytical data of gabbro (sample 499-11) from the Heiyingshan ophiolitic mélange.

Table 2. $^{40}Ar/^{39}Ar$ analytical results acquired by laser step-heating on muscovite from

the mylonitic pyllite in the matrix of the Heiyingshan ophiolitic mélange.

Table 3. Chemical compositions of magmatic rocks in the Heiyingshan mélange.

Table 4. Sr-Nd isotopic compositions of magmatic rocks from the Heiyingshan ophiolitic mélange.

Figure 1

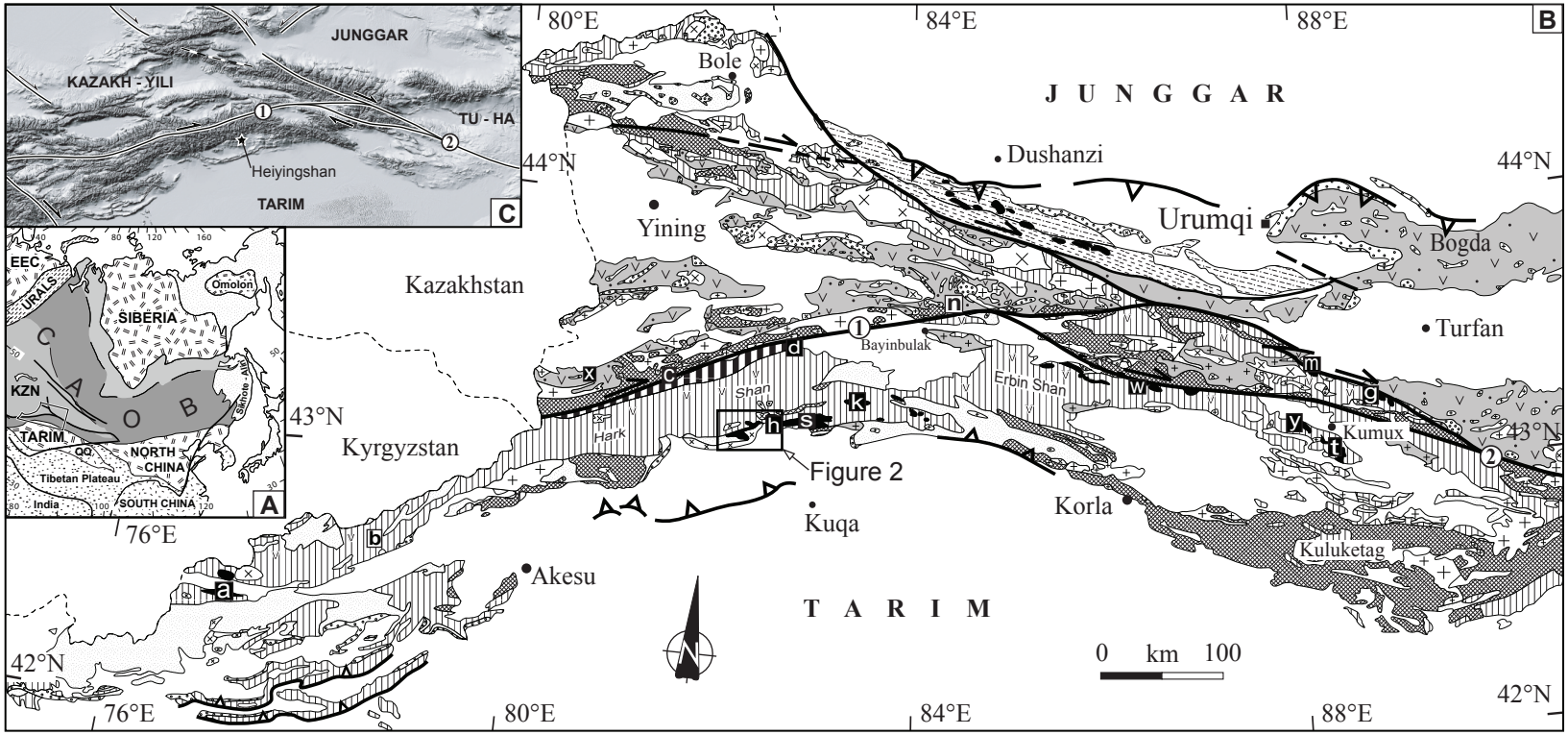

Mesozoic & Cenozoic
Permian magmatic rocks
Permian sediments
Late Paleozoic granitoids
Early Paleozoic granitoids
Late Devonian-Carboniferous volcanic & sedimentary rocks
Carboniferous sediments
Undeformed / Ductily deformed North Tianshan turbidite
Ophiolitic mélange
High pressure morphic complex
Cambrian-Devonian (volcanic interlayer)
Precambrian rocks
Cenozoic thrust
Inferred fault
Indistinct fault
Permian strike-slip fault

Figure 2

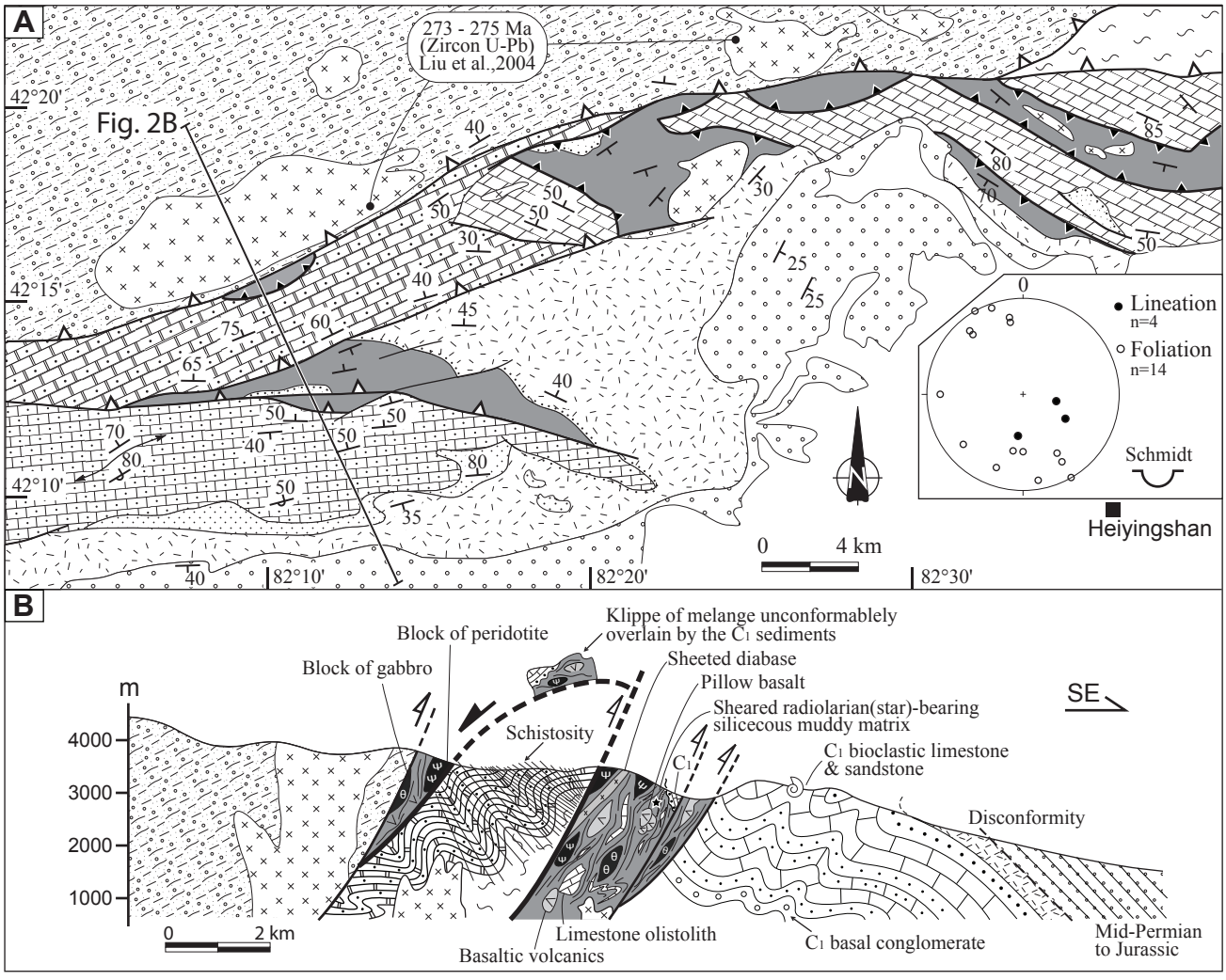
A
273 - 275 Ma
(Zircon U-Pb)
Liu et al.,2004
Fig. 2B
42°20'
42°15'
42°10'
82°10'
82°20'
82°30'
0
4 km
Lineation
n=4
Foliation
n=14
Schmidt
Heiyingshan
B
Klippe of melange unconformablely overlain by the C1 sediments
Block of peridotite
Block of gabbro
Sheeted diabase
Pillow basalt
Sheared radiolarian(star)-bearing silicecous muddy matrix
Schistosity
C1 bioclastic limestone & sandstone
Disconformity
SE
m
4000
3000
2000
1000
0
2 km
Basaltic volcanics
Limestone olistolith
C1 basal conglomerate
Mid-Permian to Jurassic
Middle Permian-Jurassic strata
Early Permian basaltic & felsic volcanic rocks
Early Permian alkaline plutonic rocks
Upper Carboniferous clastic rocks
Lower Carboniferous carbonate, clastic rocks
Ophiolitic melange
Late Silurian schistose limestone
Silurian-Ordovician marble & sandstone
Neoproterozoic (?) marble, paragneiss, cordierite quartz schist and micaschist
Proterozoic pegmatite
Pre-Permian thrust
Post Permian thrust
Anticline
Unconformity
Normal bedding
Overturned bedding

Figure 3

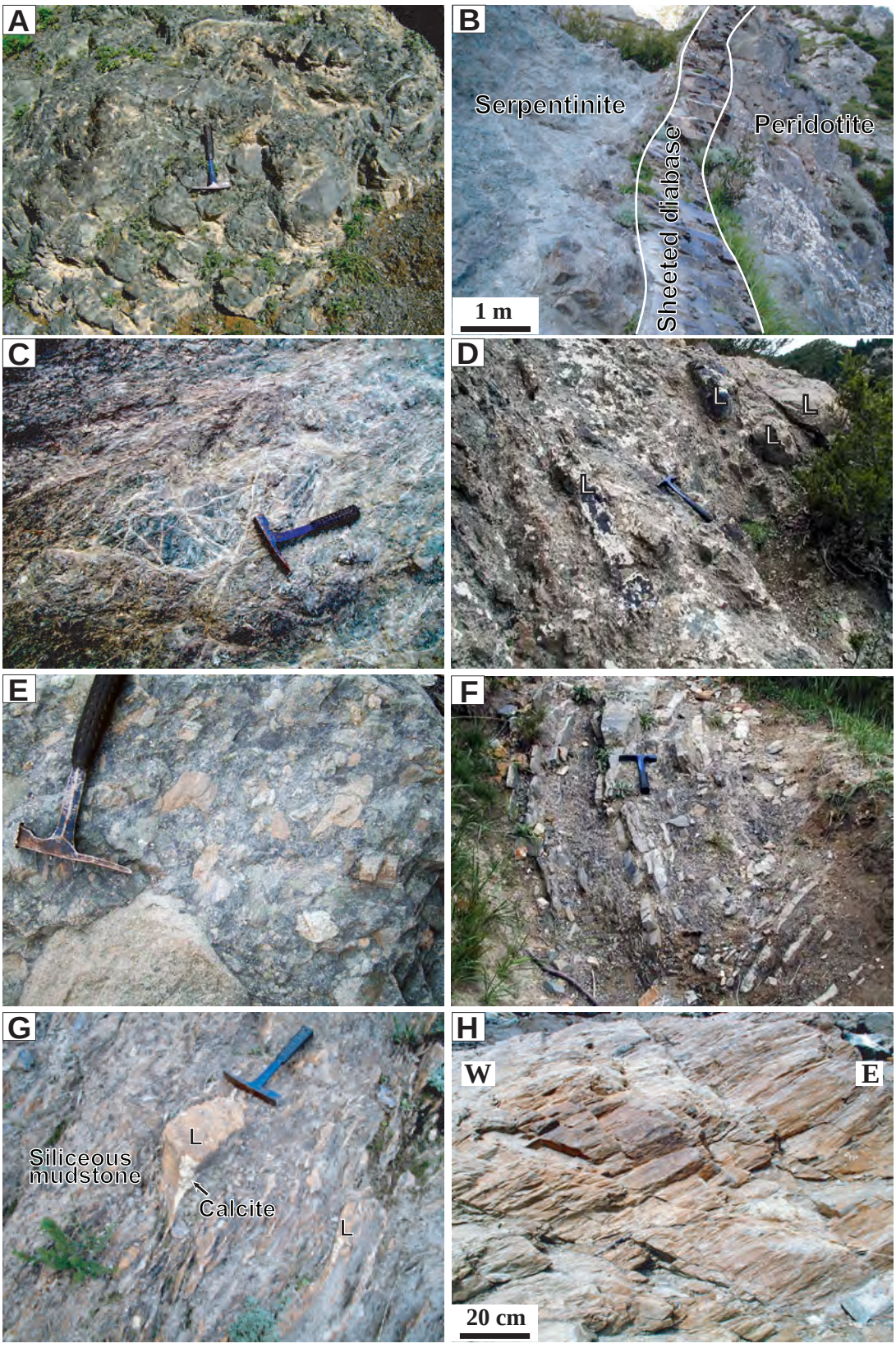
A
B
Serpentinite
Peridotite
Sheeted diabase
1 m
C
D
L
L
L
L
E
F
G
L
Siliceous mudstone
Calcite
L
H
W
E
20 cm

Figure 4

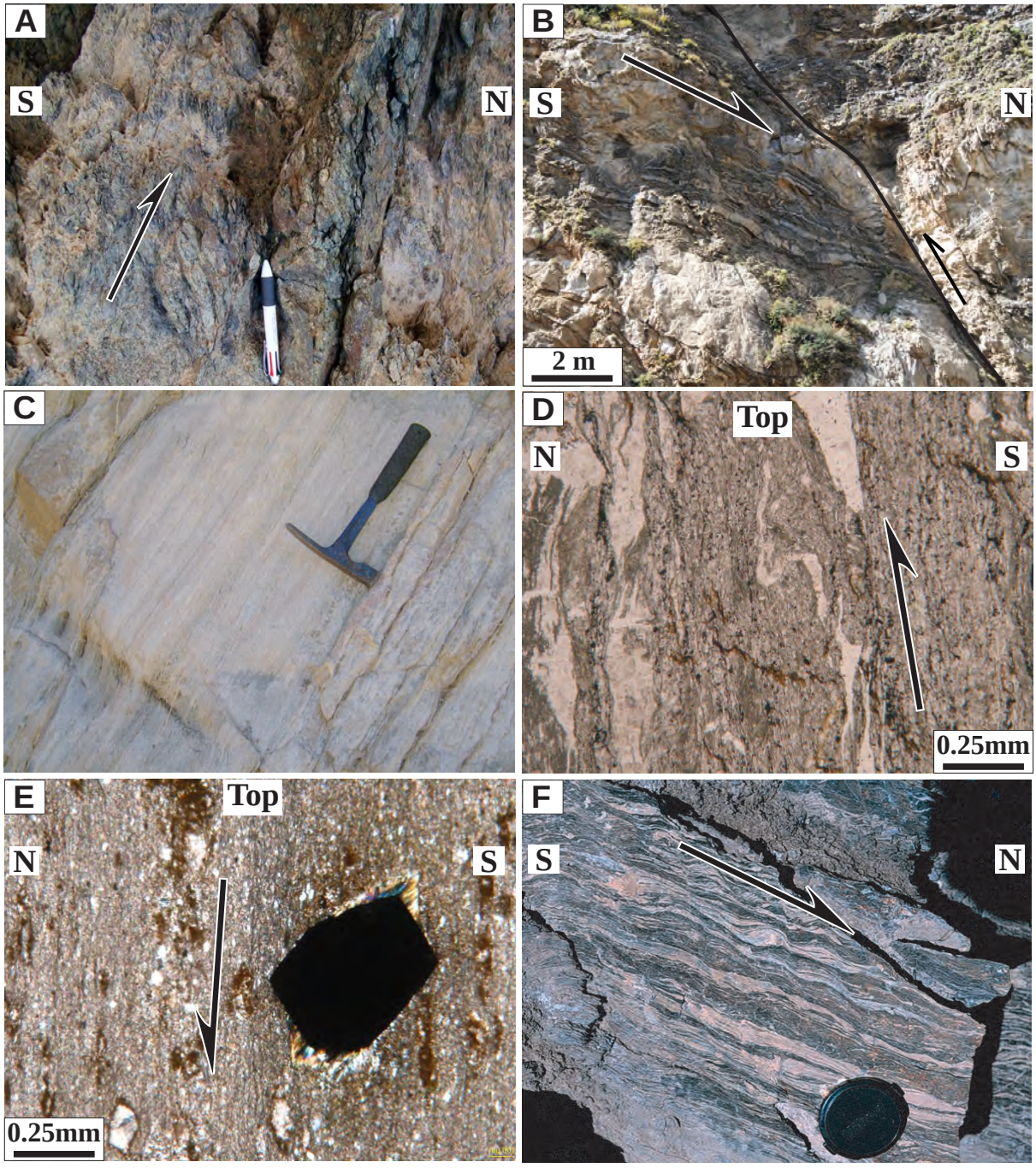

Figure 5

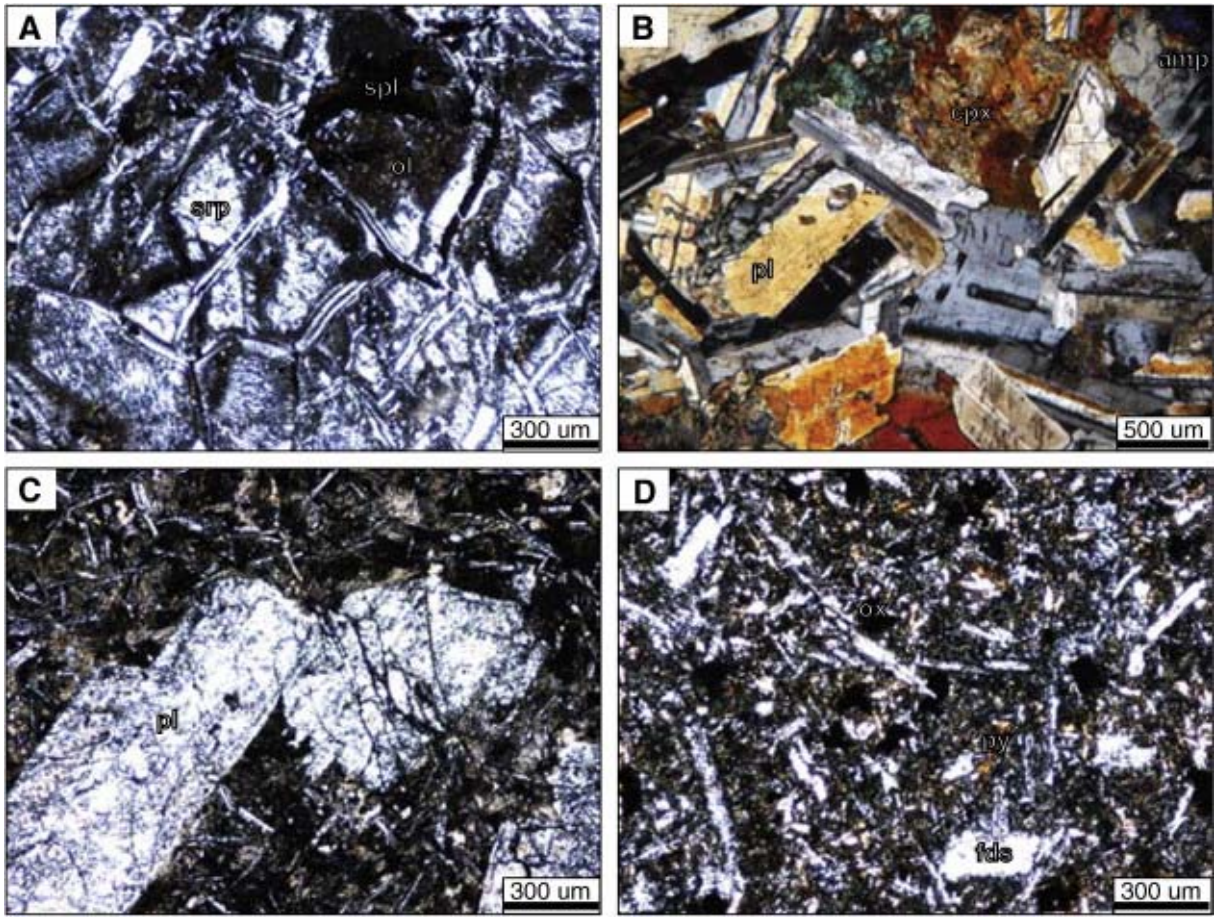
A
spl
ol
srp
300 um
B
amp
cpx
pl
500 um
C
pl
300 um
D
ox
opy
fds
300 um

Figure 6

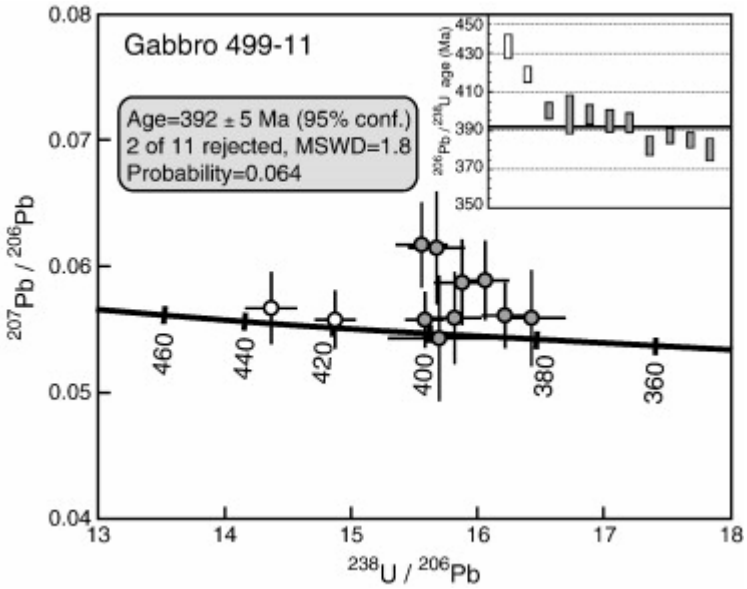
Gabbro 499-11
Age=392 ± 5 Ma (95% conf.)
2 of 11 rejected, MSWD=1.8
Probability=0.064
^{207}Pb / ^{206}Pb
^{238}U / ^{206}Pb
^{206}Pb / ^{238}U age (Ma)
0.08
0.07
0.06
0.05
0.04
13
14
15
16
17
18
460
440
420
400
380
360
450
430
410
390
370
350

Figure 7

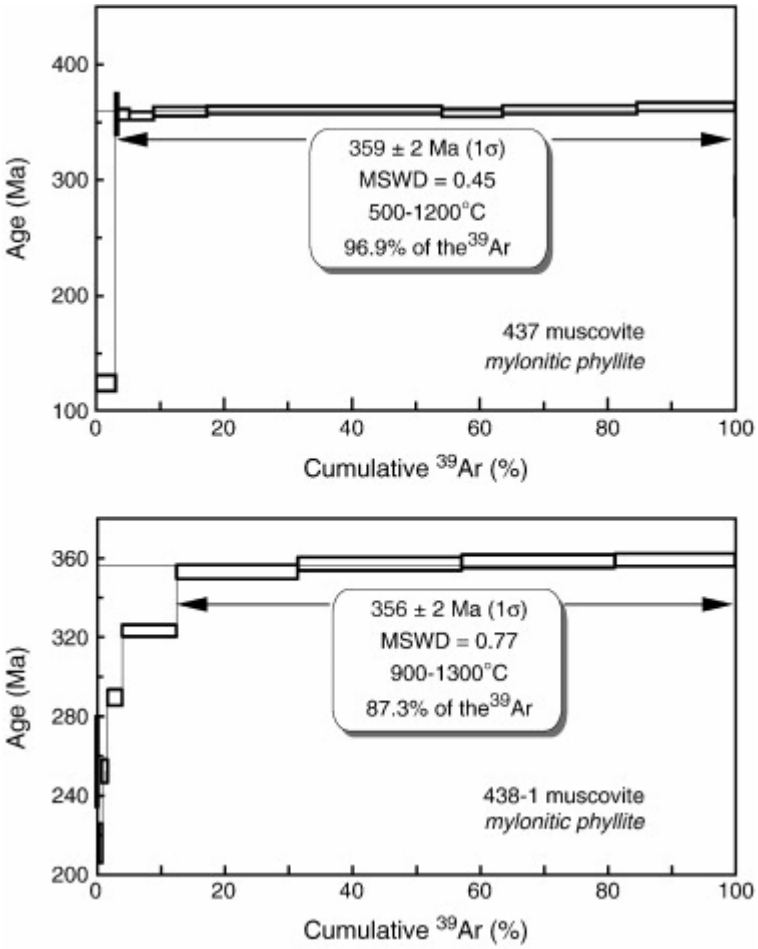
400
300
200
100
Age (Ma)
359 ± 2 Ma (1σ)
MSWD = 0.45
500-1200°C
96.9% of the 39Ar
437 muscovite
mylonitic phyllite
0
20
40
60
80
100
Cumulative 39Ar (%)
360
320
280
240
200
Age (Ma)
356 ± 2 Ma (1σ)
MSWD = 0.77
900-1300°C
87.3% of the 39Ar
438-1 muscovite
mylonitic phyllite
0
20
40
60
80
100
Cumulative 39Ar (%)

Figure 8

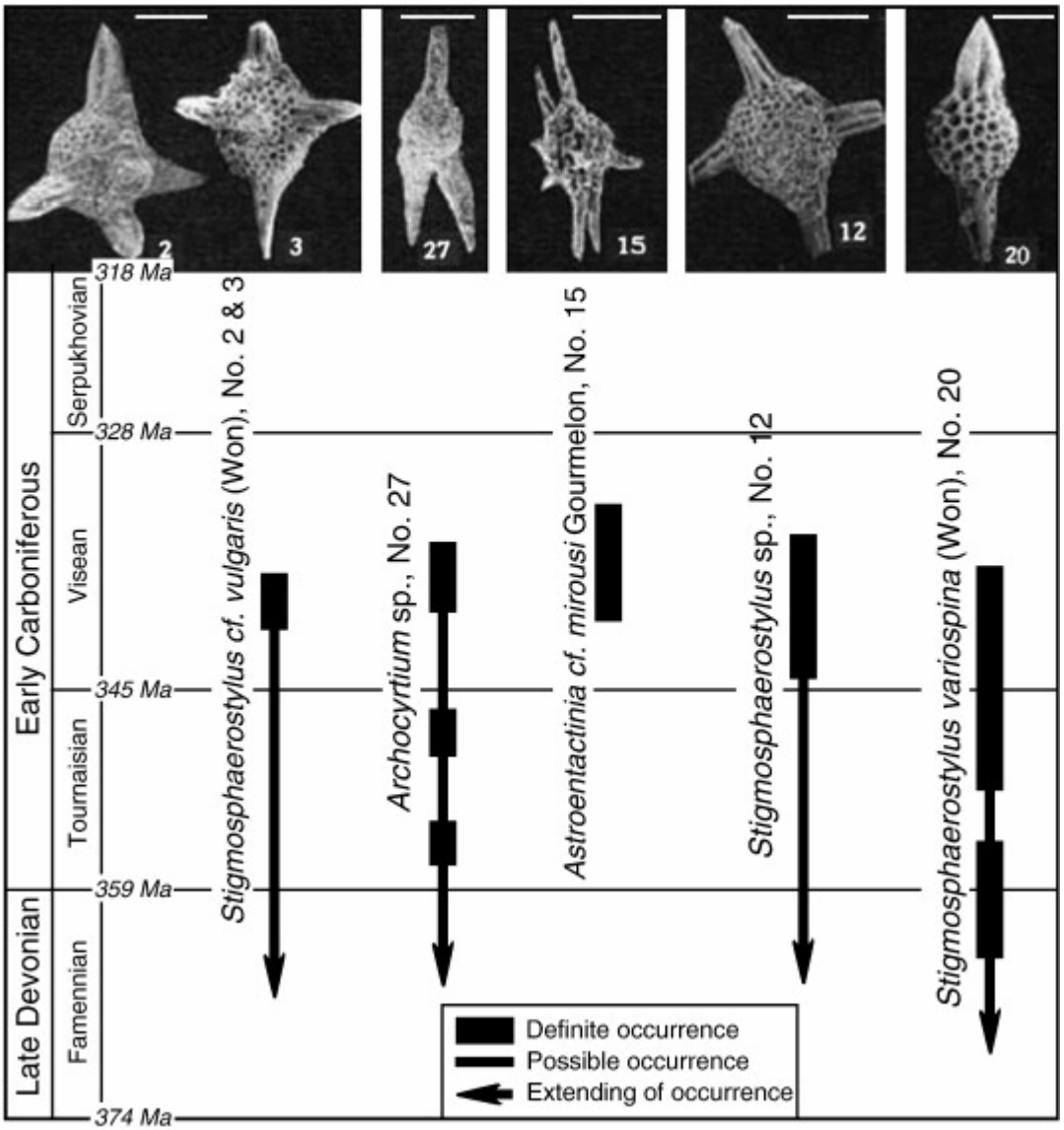
2
3
27
15
12
20
Late Devonian
Early Carboniferous
Famennian
Tournaisian
Visean
Serpukhovian
318 Ma
328 Ma
345 Ma
359 Ma
374 Ma
Stigmosphaerostylus cf. vulgaris (Won), No. 2 & 3
Archocyrtium sp., No. 27
Astroentactinia cf. mirousi Gourmelon, No. 15
Stigmosphaerostylus sp., No. 12
Stigmosphaerostylus variospina (Won), No. 20
Definite occurrence
Possible occurrence
Extending of occurrence

Figure 9

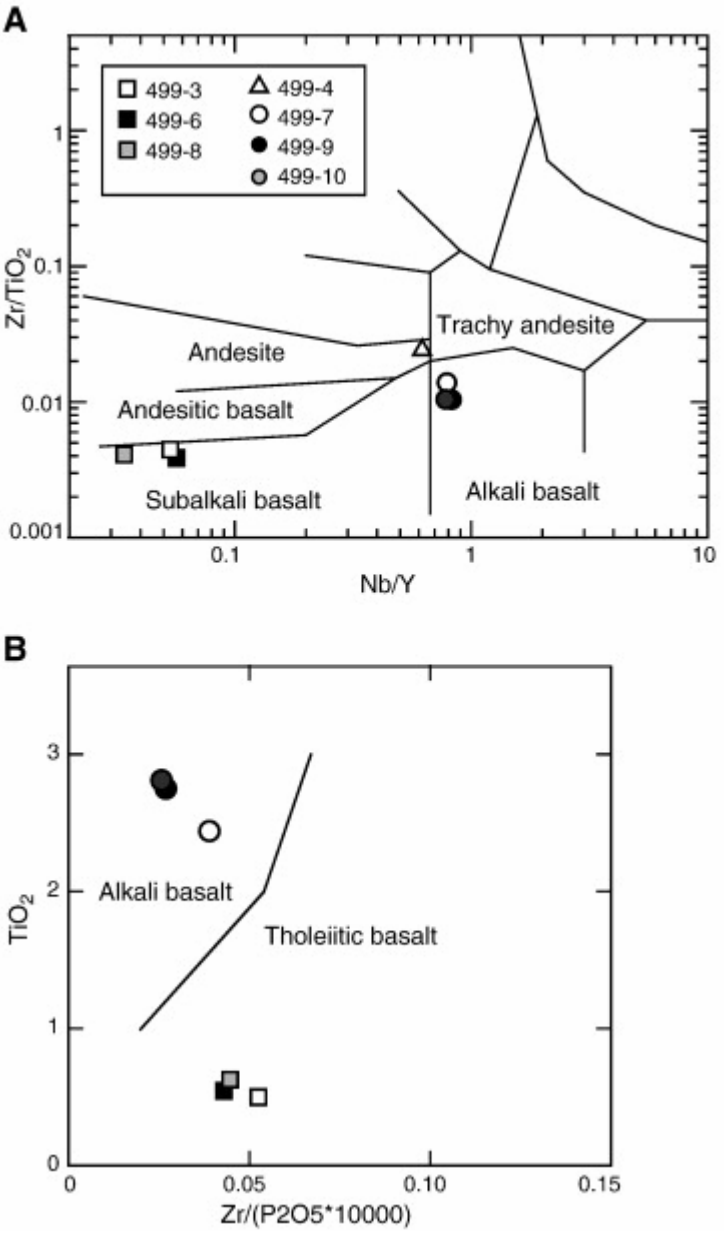
A
499-3
499-6
499-8
499-4
499-7
499-9
499-10
Zr/TiO2
Nb/Y
Trachy andesite
Andesite
Andesitic basalt
Subalkali basalt
Alkali basalt
1
0.1
0.01
0.001
0.1
1
10
B
TiO2
Zr/(P2O5*10000)
Alkali basalt
Tholeiitic basalt
3
2
1
0
0
0.05
0.10
0.15

Figure 10

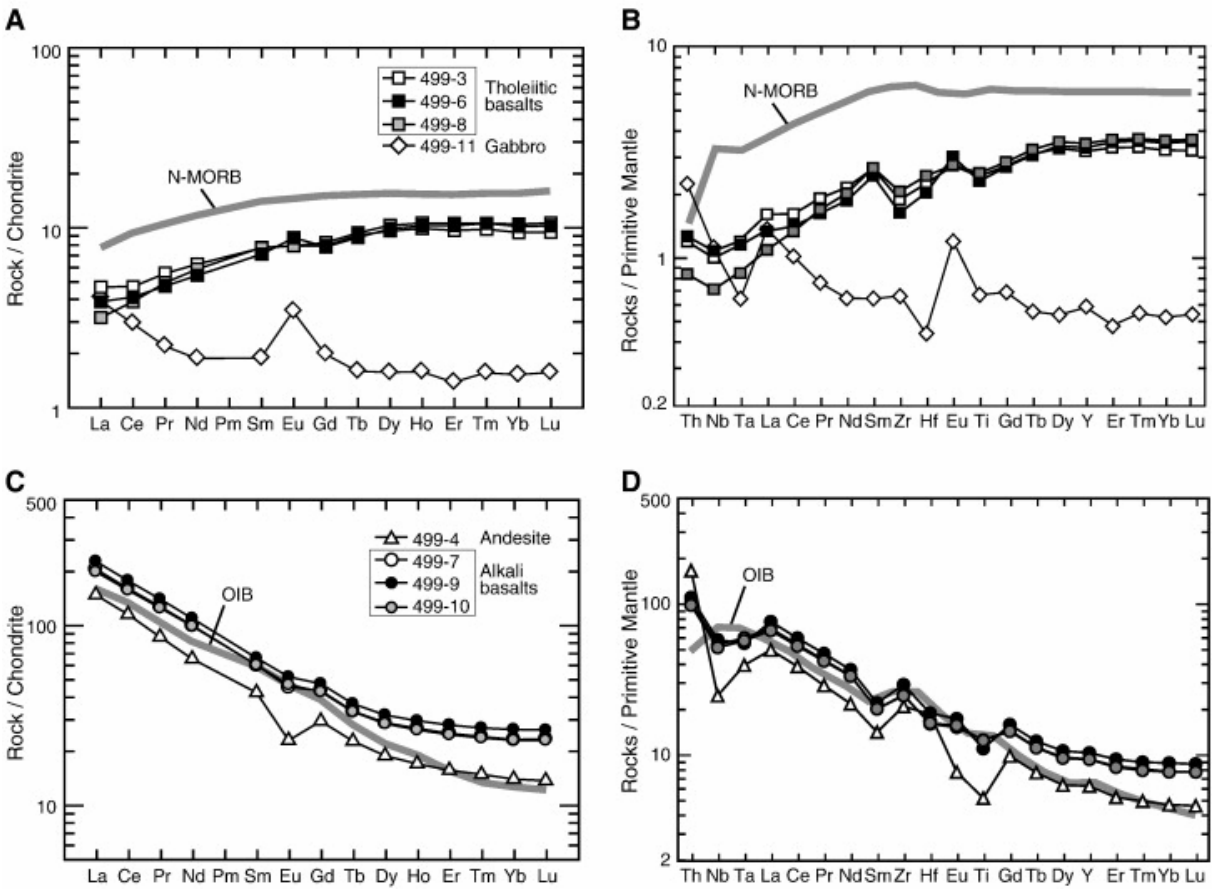

Figure 11

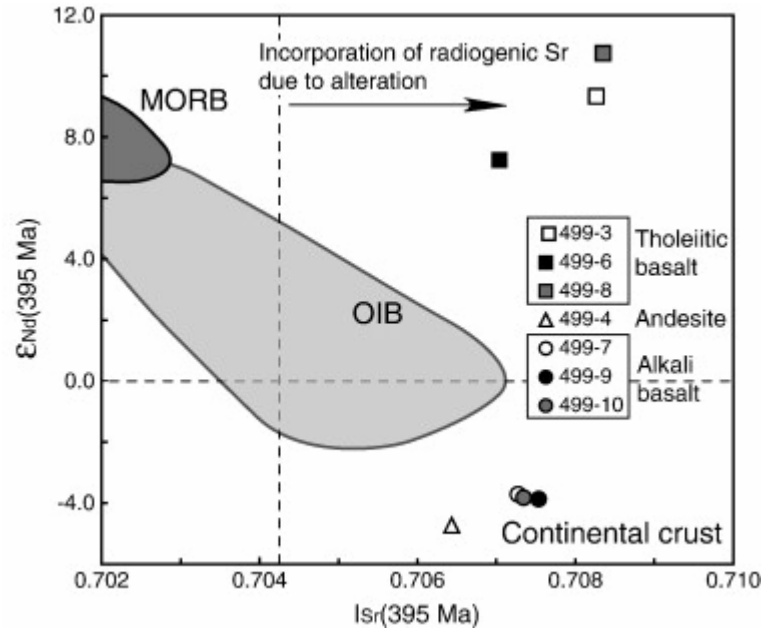

Figure 12

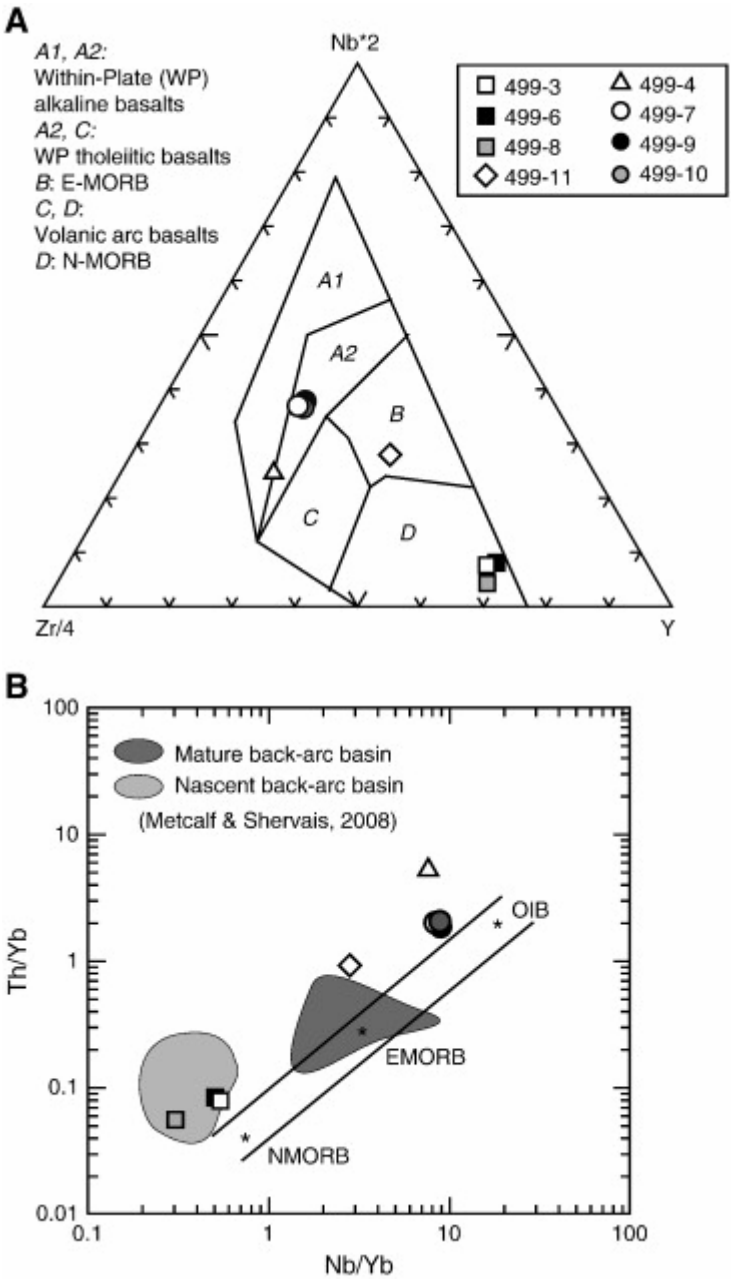
A
A1, A2:
Within-Plate (WP)
alkaline basalts
A2, C:
WP tholeiitic basalts
B: E-MORB
C, D:
Volanic arc basalts
D: N-MORB
Nb*2
Zr/4
Y
499-3
499-4
499-6
499-7
499-8
499-9
499-11
499-10
A1
A2
B
C
D
B
Mature back-arc basin
Nascent back-arc basin
(Metcalf & Shervais, 2008)
OIB
EMORB
NMORB
Th/Yb
Nb/Yb
100
10
1
0.1
0.01
0.1
1
10
100

Figure 13

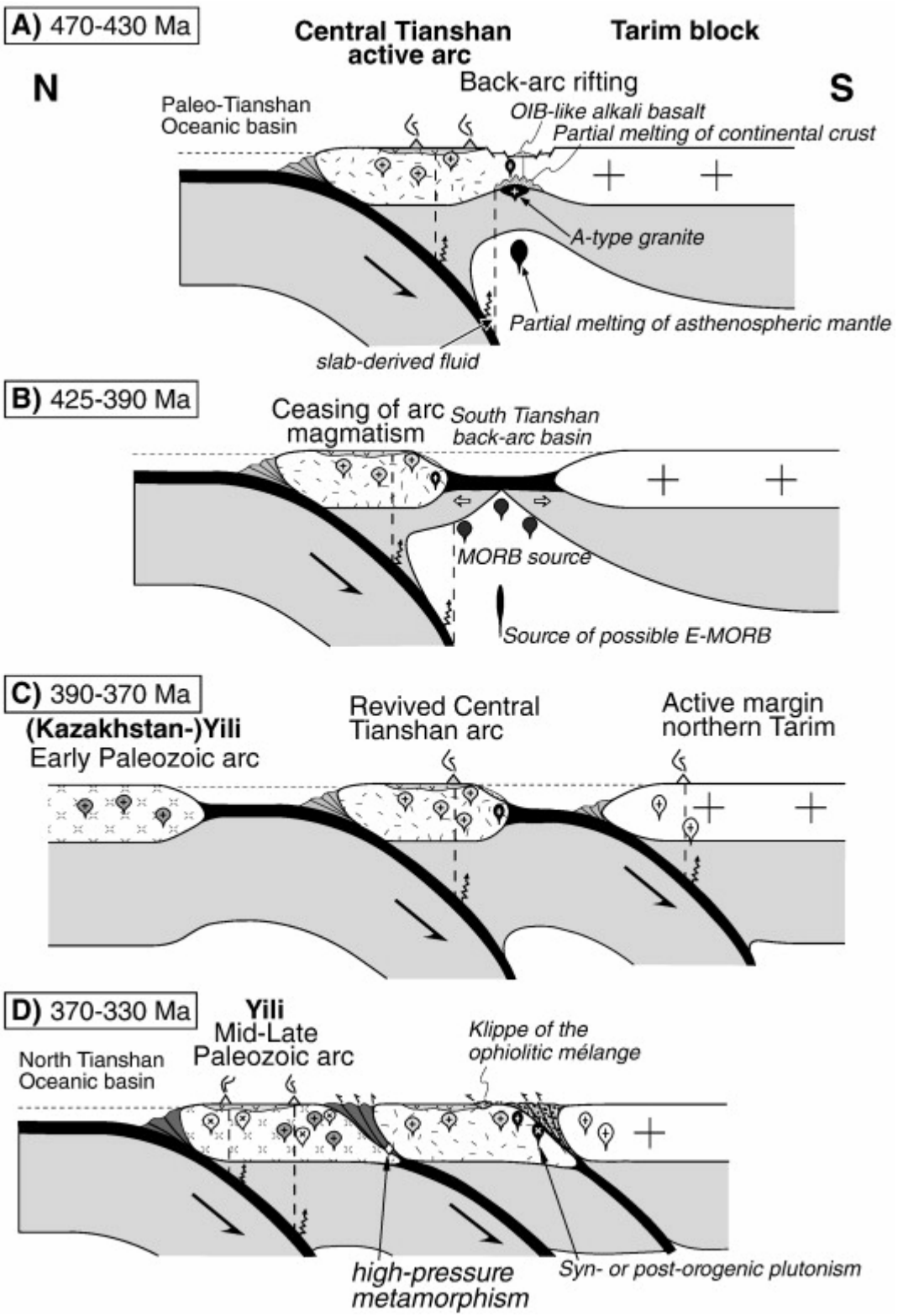
A) 470-430 Ma
Central Tianshan active arc
Tarim block
N
S
Back-arc rifting
Paleo-Tianshan Oceanic basin
OIB-like alkali basalt
Partial melting of continental crust
A-type granite
Partial melting of asthenospheric mantle
slab-derived fluid
B) 425-390 Ma
Ceasing of arc magmatism
South Tianshan back-arc basin
MORB source
Source of possible E-MORB
C) 390-370 Ma
(Kazakhstan-)Yili
Early Paleozoic arc
Revived Central Tianshan arc
Active margin northern Tarim
D) 370-330 Ma
Yili
Mid-Late Paleozoic arc
Klippe of the ophiolitic mélange
North Tianshan Oceanic basin
high-pressure metamorphism
Syn- or post-orogenic plutonism

TABLE 1. ZIRCON U-PB LA-ICPMS ANALYTICAL DATA OF GABBRO (SAMPLE 499-11) FROM THE HEIYINGSHAN MELANGE

Analyses	U	1σ	Th	1σ	Pb	1σ	Th	Atomic ratios						Apparent ages in Ma						Disc.
	(ppm)		(ppm)		(ppm)		U	$^{206}Pb/^{238}U$	1σ	$^{207}Pb/^{235}U$	1σ	$^{207}Pb/^{206}Pb$	1σ	$^{206}Pb/^{238}U$	1σ	$^{207}Pb/^{235}U$	1σ	$^{207}Pb/^{206}Pb$	1σ	(%)*
1	170	10	364	20.9	16	1	2.15	0.061	0.001	0.45	0.03	0.056	0.004	381	6	374	21	451	146	6
2	348	16	697	35.7	32	2	2.01	0.062	0.001	0.44	0.02	0.056	0.002	386	4	373	14	460	98	4
3	306	15	591	29.3	28	1	1.93	0.062	0.001	0.47	0.02	0.059	0.003	389	4	390	17	564	113	4
4	210	10	557	26.6	22	1	2.65	0.063	0.001	0.47	0.03	0.059	0.003	394	5	393	19	559	122	5
5	320	17	572	31.3	28	2	1.79	0.063	0.001	0.45	0.03	0.056	0.004	395	5	380	20	451	140	5
6	459	34	802	59.4	41	3	1.75	0.064	0.001	0.51	0.04	0.062	0.004	399	5	420	24	657	152	6
7	417	18	636	28.7	37	2	1.53	0.064	0.001	0.51	0.03	0.062	0.003	402	5	420	18	665	114	5
8	358	18	697	36.6	33	2	1.95	0.064	0.002	0.46	0.04	0.054	0.005	398	10	386	26	386	201	10
9	601	27	1585	74.6	65	3	2.64	0.064	0.001	0.46	0.02	0.056	0.002	401	4	381	12	446	84	4
10	441	20	859	41.7	43	2	1.95	0.067	0.001	0.48	0.02	0.056	0.002	419	4	398	14	446	87	4
11	269	12	179	8.4	21	1	0.67	0.070	0.001	0.52	0.03	0.057	0.003	434	6	422	18	482	108	6

Note: Analyses done at the School of Earth Sciences, University of Tasmania (Australia).

* Disc. (%) denotes percentage of discordance.

TABLE 2. $^{40}AR/^{39}AR$ ANALYTICAL RESULTS ACQUIRED BY LASER STEP-HEATING ON THE MUSCOVITE FROM THE MYLONITIC PYLLITE IN THE METRIX OF THE HEIYINGSHAN MELANGE

Step	Temperature (°C)	$(^{40}Ar/^{39}Ar)_m$ †	$(^{36}Ar/^{39}Ar)_m$	$(^{37}Ar/^{39}Ar)_m$	$(^{38}Ar/^{39}Ar)_m$	^{40}Ar（%）	$(^{40}Ar^*/^{39}Ar)$ §	^{39}Ar ($\times10^{-14}$ mol)	^{39}Ar (Cum.)(%)	Age (Ma)	1σ (Ma)
Sample 437; J=0.005264 #; total weight of mesured muscovite is 44.57 mg											
1	400	39.5	0.088	0.138	0.037	34.4	13.6	130	3.04	124.5	6.8
2	500	120.7	0.268	0.406	0.071	34.4	41.5	14.3	3.37	357	18
3	600	57.4	0.054	0.068	0.024	72.4	41.6	77.9	5.2	356.8	4.9
4	700	49.4	0.027	0.057	0.019	83.7	41.4	161	8.97	355.4	3.5
5	800	47.7	0.020	0.014	0.018	87.7	41.9	356	17.3	359.3	4
6	900	43.4	0.005	0.007	0.015	96.7	42.0	1570	54.1	360.5	3.5
7	1000	45.9	0.014	0.013	0.018	91	41.8	403	63.5	358.4	3.5
8	1100	44.0	0.007	0.008	0.015	95.5	42.0	897	84.6	360.7	3.7
9	1200	42.8	0.001	0.018	0.014	99.1	42.4	654	99.9	363.4	3.6
10	1300	51.5	0.064	1.502	0.068	63.3	32.6	4.4	100	286	17
Sample 438-1; J=0.005345; total weight of mesured muscovite is 44.3 mg											
1	400	41.3	0.043	0.510	0.039	69.3	28.7	22.8	0.46	257	23
2	500	32.4	0.029	0.321	0.023	73.5	23.8	27.3	1.02	216	10
3	600	32.6	0.015	0.153	0.018	86.2	28.1	44.0	1.91	252.1	6
4	700	34.5	0.007	0.051	0.015	94.4	32.6	111	4.16	289.4	4
5	800	38.2	0.005	0.163	0.019	96.0	36.7	420	12.7	323.2	3.1
6	900	42.4	0.007	0.057	0.016	94.9	40.2	928	31.6	351.3	3.4
7	1000	41.8	0.003	0.024	0.014	98.0	40.9	1260	57.2	356.9	3.4
8	1100	42.1	0.003	0.020	0.014	97.6	41.1	1174	81.1	358.1	3.3
9	1200	41.7	0.002	0.029	0.014	98.8	41.2	923	99.8	358.8	3.3
10	1300	53.0	0.043	4.501	0.084	76.5	40.7	8.04	100	354.8	8.7

Note : Analyses done at the Institute of Geology, Chinese Academy of Geological Sciences.

† subscript "m" means mesured isotopic ratios.

§ $^{40}Ar^*$ is the radiogenic argon.

J is the irradiation parameter.

TABLE 3. BULK GEOCHEMISTRY OF THE MAGMATIC ROCKS IN THE HEIYINGSHAN MELANGE

Sampls	Andesite	Alkali basalts			Tholeiitic basalts			Gabbro	Peridotites	
	499-4	499-7	499-9	499-10	499-3	499-6	499-8	499-11	499-13	499-14
SiO_2 (wt%)	57.3	44.4	45.8	43.5	44.4	46.2	43.3	41.8	38.4	40.1
TiO_2	0.94	2.75	2.44	2.81	0.52	0.55	0.60	0.12	0.01	0.02
Al_2O_3	14.1	14.4	14.4	14.6	15.4	18.7	14.0	19.4	0.42	0.24
Fe_2O_3	0.43	4.78	3.78	5.66	2.04	1.93	3.51	1.19	6.80	9.06
FeO	2.57	9.29	9.32	8.63	5.51	5.96	4.51	4.61	0.90	2.16
MnO	0.07	0.19	0.20	0.19	0.14	0.12	0.15	0.08	0.08	0.05
MgO	3.92	2.14	1.71	2.20	7.63	6.84	7.41	14.6	39.4	34.9
CaO	7.41	13.0	13.6	13.4	13.5	10.6	14.2	10.2	0.11	2.20
Na_2O	5.00	2.93	1.41	2.30	3.41	2.69	3.35	0.79	0.10	0.04
K_2O	0.62	1.99	3.84	2.36	0.69	1.17	0.34	1.01	0.01	0.01
P_2O_5	0.22	1.06	0.87	1.15	0.05	0.05	0.06	0.02	0.01	0.02
LOI	6.80	2.62	2.28	2.54	6.24	4.55	8.47	6.00	12.7	10.3
Total	99.4	99.5	99.7	99.4	99.5	99.3	99.9	99.9	98.9	99.1
Mg# [†]	0.72	0.24	0.21	0.24	0.67	0.64	0.66	0.84	0.92	0.87
Sc (ppm)	13.4	6.41	5.9	6.34	36.7	28.3	35.9	8.24	9.00	6.70
Ti	6762	16390	14360	16300	3182	3017	3297	874	28.3	116
V	86.9	25.4	19.7	25.0	196	192	206	32.9	33.0	30.0
Cr	74.8	15.1	12.6	18.0	679	130	571	456	1725	2420
Mn	724	1555	1561	1442	967	907	1202	657	632	510
Co	8.95	28.8	22.7	35.6	40.3	33.7	41.5	50.1	79.9	106.3
Ni	46.8	7.86	5.45	9.1	160	55.6	138	289	1310	1220
Cu	20.6	22.3	18.8	22.8	63.5	24.9	27.8	26.5	0.3	25.0
Zn	72.6	198	189	221	56.8	59.7	62.7	19.6	19.3	20.7
Ga	25.5	23.3	23.3	22.6	11.8	14.5	11.8	10.4	0.8	1.5
Rb	13.2	39	66.8	51.4	1.65	23.2	5.64	17.04	0.37	0.36
Sr	239	311	501	408	106	165	187	188.2	5.5	5.1
Y	28.5	42.9	47.2	42.7	14.6	15.2	15.9	2.67	0.23	0.43
Zr	236	281	329	278	21.2	18.4	23.2	7.61	0.97	0.90
Nb	17.7	38.5	41.5	36.8	0.72	0.77	0.51	0.84	0.11	0.11
Mo	0.93	1.37	1.23	2.07	0.18	0.09	0.21	0.78	0.99	0.70
Cd	0.07	0.08	0.09	0.10	0.02	0.01	0.02	-	-	-
Sn	7.25	2.40	2.18	2.46	0.28	0.27	0.23	0.16	0.19	0.23
Cs	0.24	0.22	0.36	0.45	0.28	1.62	0.43	0.30	0.09	0.09
Ba	223	644	1290	1036	47.6	443	102	118.9	6.8	5.1
La	34.2	47.6	52.6	46.0	1.11	0.92	0.75	0.94	0.35	0.18
Ce	68.8	96.0	106.0	93.9	2.88	2.52	2.38	1.81	0.63	0.35
Pr	8.0	11.8	13.0	11.6	0.53	0.45	0.47	0.21	0.07	0.04
Nd	29.7	45.6	49.9	45.2	2.93	2.54	2.75	0.88	0.23	0.15
Sm	6.32	8.99	9.85	9.01	1.18	1.09	1.19	0.29	0.05	0.05
Eu	1.30	2.57	2.93	2.65	0.46	0.51	0.46	0.20	0.05	0.02
Gd	5.90	8.71	9.52	8.59	1.63	1.61	1.70	0.41	0.04	0.04
Tb	0.83	1.22	1.34	1.21	0.34	0.33	0.35	0.06	0.01	0.01
Dy	4.68	7.14	7.88	7.05	2.44	2.51	2.62	0.40	0.03	0.05
Ho	0.94	1.48	1.63	1.45	0.56	0.58	0.60	0.09	0.01	0.01
Er	2.53	4.06	4.52	3.99	1.60	1.70	1.75	0.23	0.02	0.05
Tm	0.37	0.60	0.67	0.59	0.25	0.27	0.27	0.04	0.00	0.01
Yb	2.32	3.85	4.38	3.82	1.60	1.73	1.78	0.26	0.03	0.07
Lu	0.34	0.58	0.65	0.57	0.24	0.26	0.27	0.04	0.01	0.02
Hf	5.79	4.99	5.87	5.05	0.70	0.63	0.76	0.13	0.02	0.03
Ta	1.62	2.45	2.26	2.35	0.05	0.05	0.04	0.03	0.01	0.03
W	2.23	0.75	1.24	1.10	0.14	0.22	0.16	0.30	0.29	0.38
Pb	22.7	15.3	17.5	15.9	0.22	0.20	0.51	0.48	0.05	0.55
Th	14.20	8.68	9.40	8.37	0.10	0.11	0.07	0.19	0.04	0.04
U	7.64	2.47	2.55	2.37	0.06	0.06	0.05	0.05	0.52	0.11
Eu_N/Eu^* [§]	0.65	0.89	0.93	0.92	1.02	1.17	1.00	1.79	3.90	1.54
$(La/Sm)_N$	3.5	3.4	3.4	3.3	0.6	0.5	0.4	2.1	4.9	2.4
$(La/Yb)_N$	10.6	8.9	8.6	8.6	0.5	0.4	0.3	2.6	7.8	1.7
Zr/Nb	13.3	7.3	7.9	7.6	29.6	23.8	45.6	9.0	8.6	8.2
Zr/Hf	40.8	56.3	56.0	55.0	30.4	29.1	30.6	58.8	53.8	29.9
$(Th/Nb)_n$ [††]	6.7	1.9	1.9	1.9	1.2	1.2	1.2	1.9	3.3	2.8
Nb/Ta	10.9	15.7	18.4	15.7	13.5	14.3	12.8	32.0	15.0	4.1

Note: REE and trace elements of gabbro and peridotites and all major elements were analyzed at Nanjing University; the REE and trace elements of the andesite of basalts were analyzed at National Taiwan University.

[†] Mg# = MgO/(MgO+0.505×(Fe_2O_3×0.9+FeO)) assuming that FeO equals to 90% of total Fe-oxide.

[§] $Eu^* = (Sm_N \times Gd_N)^{1/2}$; N: normalization to Chondrites (Sun and McDonough, 1989).

[††] n: normalization to Primitive Mantle (Sun and McDonough, 1989).

TABLE 4. SR-ND ISOTOPIC COMPOSITIONS OF THE MAGMATIC ROCKS FROM THE HEIYINGSHAN OPHIOLITIC MELANGE

Samples	Rocks	Age* (Ma)	Rb (ppm)	Sr (ppm)	$^{87}Rb/^{86}Sr$	$^{87}Sr/^{86}Sr$	$2\sigma_m$	$I_{Sr}(T)$	Sm (ppm)	Nd (ppm)	$^{147}Sm/^{144}Nd$	$^{143}Nd/^{144}Nd$	$2\sigma_m$	$\varepsilon_{Nd}(0)$	$\varepsilon_{Nd}(T)$	$f_{Sm/Nd}$ †	T_{DM-1} § (Ma)	T_{DM-2} # (Ma)
449-4	andesite	395	13.2	239	0.160	0.707324	10	0.70643	6.32	29.7	0.1287	0.512222	8	-8.1	-4.7	-0.35	1661	1500
449-7	alkali basalt	395	39	311	0.363	0.709292	10	0.70727	8.99	45.6	0.1192	0.512250	7	-7.6	-3.7	-0.39	1450	1442
449-9	alkali basalt	395	66.8	501	0.386	0.709679	12	0.70754	9.85	49.9	0.1193	0.512242	5	-7.7	-3.9	-0.39	1464	1455
449-10	alkali basalt	395	51.4	408	0.365	0.709373	11	0.70734	9.01	45.2	0.1206	0.512248	7	-7.6	-3.8	-0.39	1475	1447
449-3	Tholeiite	395	1.65	106	0.045	0.708518	11	0.70827	1.18	2.93	0.2436	0.513236	6	11.7	9.3	0.24	440	-
449-6	Tholeiite	395	23.2	165	0.408	0.709305	9	0.70704	1.09	2.54	0.2601	0.513171	8	10.4	7.2	0.32	69	-
449-8	Tholeiite	395	5.64	187	0.087	0.708839	7	0.70835	1.19	2.75	0.2621	0.513356	6	14.0	10.7	0.33	648	-

Note: Analyses done at the Institute of Earth Sciences, Academia Sinica (Taipei).

* Ages are given assuming that the volcanic rocks formed synchronously with or a little earlier than the gabbro that is dated at 392± 5 Ma.

† $f_{Sm/Nd}$ (fractionation factor) = $[(^{147}Sm/^{144}Nd)_s/(^{147}Sm/^{144}Nd)_{CHUR}]-1$.

§ T_{DM-1} (single-stage model age) = $1/\lambda \ln\{1+[(^{143}Nd/^{144}Nd)_s-0.51315]/[(^{147}Sm/^{144}Nd)_s-0.2137]\}$, where s stands for sample, $\lambda = 0.00654\ Ga^{-1}$ is the decay constant of ^{147}Sm.

\# T_{DM-2} (two-stage model age) = $T_{DM-1}-(T_{DM-1}-t)(f_{cc}-f_s)/(f_{cc}-f_{DM})$, where f_{cc}, f_s and f_{DM} are $f_{Sm/Nd}$ values of the average continental crust, sample and the depleted mantle, respectively. In this study, $f_{cc} = -0.4$ and $f_{DM} = 0.08592$ are used. The t is the age of the rocks.